Investigating Acute Microglia Response to Seizure Activity *in Vivo*: Combining 2-Photon Imaging and EEG Recording

by

Julie Murmann

April, 2024

A thesis submitted to the
Graduate School
of the
Institute of Science and Technology Austria
in partial fulfillment of the requirements
for the degree of
Master of Science

Committee in charge:
Dr. Sandra Siegert
Dr. Johann Danzl

The thesis of Julie Murmann, titled *Investigating Acute Microglia Response to Seizure Activity in Vivo: Combining 2-Photon Imaging and EEG Recording* is approved by:

Supervisor: Sandra Siegert, ISTA, Klosterneuburg, Austria

Signature: _____

Committee Member: Johann Danzl, ISTA, Klosterneuburg, Austria

Signature: _____

Signed page is on file

ISTA Master's Thesis, ISSN: 2791-4585

I hereby declare that this thesis is my own work and that it does not contain other people's work without this being so stated; this thesis does not contain my previous work without this being stated, and the bibliography contains all the literature that I used in writing the dissertation.

I accept full responsibility for the content and factual accuracy of this work, including the data and their analysis and presentation, and the text and citation of other work.

I declare that this is a true copy of my thesis, including any final revisions, as approved by my thesis committee, and that this thesis has not been submitted for a higher degree to any other university or institution.

I certify that any republication of materials presented in this thesis has been approved by the relevant publishers and co-authors.

Signature: _____

Julie Murmann

April, 2024

Signed page is on file

Abstract

Epilepsy affects about 50 to 65 million people globally. It summarizes a spectrum of neurological disorders that have in common a hyperactivity of the neuronal network resulting in seizures. A common assumption is that an imbalance between neuronal excitation and inhibition is a key mechanism in seizure generation and epileptogeneisis. In at least one-third of the patients, current therapies have proven unsuccessful in treating seizure progression. One potential reason could be that the therapies only focus on neurons. Recent studies suggest that neuronal hyperactivity causes a microglial response, which reinstates brain homeostasis. Additionally, interactions between microglia and neurons have been shown to inhibit neuronal firing and dampen seizure activity. However, the exact relationship between microglia and seizure progression in epilepsy is yet to be elucidated. A main bottleneck is that several studies investigate microglia dynamics in *ex vivo* slice models, which can severely affect the microglia dynamics due to their rapid response to environmental changes. On the other hand, *in vivo* studies focus mostly on behavior characterization of the epileptic seizure phenotype and their long-term consequences on microglia activity leaving out the direct consequences of acute seizure activity on microglia dynamics.

Here, we perform a pilot study to combine electroencephalography (EEG) and *in vivo* live imaging to directly monitor and correlate the onset of seizure activity with microglia response. To induce seizures, we take advantage of the kainic acid (KA) model, which represents similar neuropathological and electroencephalographic features seen in human patients with temporal lobe epilepsy (TLE). After confirmation of induction of the seizure and microglia activity in the hippocampus as a focal point, we investigated whether these changes also reached the primary visual cortex (V1) as a secondary generalized seizure activity. Indeed, we found that microglia changed their morphology at high doses of KA in the V1. Next, we optimized each of the two methodological components: for the EEG recording, our initial attempts under the microscope suffered from extensive electrical noise, which overlaid the actual signal. Thus, we built a customized Faraday-cage and confirmed that the signal-to-noise ratio was sufficiently reduced to be able to record brain oscillatory activity. For the *in vivo* live imaging of microglia, we had to optimize the imaging parameters, so that we would be able to detect microglial processes in a sufficient resolution to track their process changes. Finally, we combined both methodologies with the KA model. We confirmed that KA induced seizure activity and found first indication that those correlate with microglia volume changes.

Overall, we have developed a first methodological approach, which allows the analysis of the acute effects of seizure onset on microglia. Future studies will have to continue to optimize the drift during imaging recording and the post-image analysis.

Acknowledgments

I would like to first sincerely thank Dr. Sandra Siegert for giving me the opportunity to work in her laboratory and to perform my master's project. This was a unique situation, and she made sure that I took the best out of the situation.

Furthermore, I would like to thank Alessandro Venturino for supervising me. Without his constant help and support this would not have been possible. His humor and patience helped me through the times where I wasn't sure how to proceed. I would also like to thank Amin Alamalhoda for helping with my project. His knowledge and support is irreplaceable. Natalie Özgen and Fleur Uiterkamp, you two were my office partners and friends outside of work. Thank you for your support and for listening to me and sharing your own stories.

Additionally, I would like to thank the rest of the Siegert Lab for their kindness and support. Every single one of you is an amazing person and gave me advice and encouragement during my many doubtful moments.

My gratitude also goes to the Imaging and Optics Facility, specifically Mohammad Goudarzi, the Lab Support Facility as well as the Preclinical facility of ISTA for their services and assistance. Additionally, I am thankful to the Machine Shop for their invaluable support in constructing various components essential to my project.

Thank you also of course goes to my two roommates, Sima and Lenka. We started this program together, and have become close friends. Without their support at home, and a quick chat over tea, I don't know what I would have done.

Finally thank you to my family, whom I don't get to see very often, but who are there if I need them, and my mom, who will answer the phone even if it's 5 am in Chicago.

About the Author

Julie Murmann complete a BSc in Behavioral Neuroscience at Northeastern University in Boston, Massachusetts before joining ISTA in September 2021. During her studies she had two six month research internships, one at Harvard Medical School in Boston, Massachusetts, and the other at NERF in Leuven, Belgium, both in systems neuroscience fields.

These two experiences lead to her interest in systems neuroscience, and brought her to the ISTA PhD program. There she discovered and interest in cellular neuroscience and microglia. During her first year of PhD studies, a decision was made to graduate from ISTA with an MSc degree focusing on microglia-neuron interactions

Table of Contents

List of Figures

List of Tables

List of Abbreviations

2P 2-photon

BBB blood brain barrier

CNS central nervous system

DG dentate gyrus

EEG Electroencephalography

EMG Electromyography

FrL left frontal lobe

FrR right frontal lobe

GND ground

i.p. *intraperitoneal*

Iba1 Ionized calcium binding adaptor molecule 1

KA kainic acid

Occ occipital lobe

PBS phosphate buffered saline

PFA paraformaldehyde

RT room temperature

s.c. *subcutaneous*

SE *status epilepticus*

TLE temporal lobe epilepsy

V1 primary visual cortex

WT wildtype

1. Introduction

1.1 Epilepsy

Epilepsy summarizes a spectrum of neurological disorders that have in common a predisposition to hyper-synchronous neuronal activity in the form of seizures. At least one seizure is required to establish the presence of epilepsy (Fisher et al., 2005). Seizures are abnormal, synchronous excitation of a neuronal population that typically lasts seconds or minutes (Scharfman, 2007).

Epilepsy affects about 50 to 65 million people globally (Thurman et al., 2011), including both children and adults. Patients with epilepsy experience a higher mortality rate with an estimated 2-10 years earlier than the general population (Gaitatzis et al., 2004). Epilepsy is the fourth most common neurological disorder worldwide (Sharma et al., 2019), with temporal lobe epilepsy (TLE) being the most common type of epilepsy (Engel, 2001). TLE consists of partial seizures that originate from the hippocampus, entorhinal cortex or amygdala years after an initial injury, encephalitis or febrile convulsions (Lévesque and Avoli, 2013). After this initial injury there is a period without evidence of overt seizures, after which recurrent seizures begin (**Figure 1**) (Scharfman, 2007).

Although there are many antiepileptic drugs available, they have been unsatisfying and proven to be unsuccessful in at least one-third of patients (Eyo et al., 2017; Engel et al., 2012).

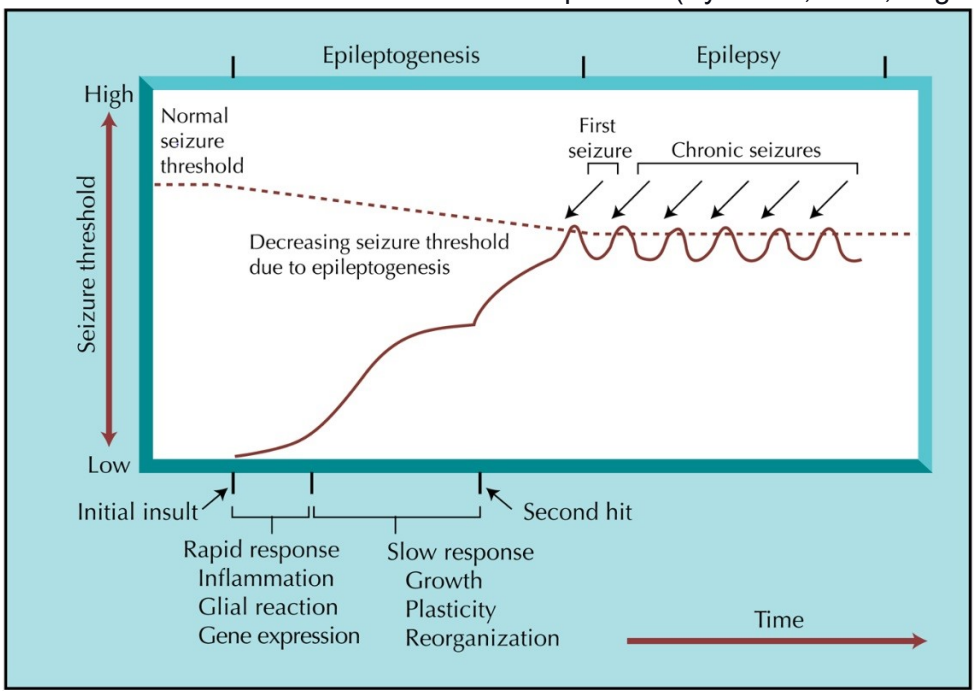

Figure 1: description on page 7.

Figure 1: A timeline for epileptogenesis in temporal lobe epilepsy. "Acquired epilepsy, using temporal lobe epilepsy as an example, can be simplified as three stages: an initial insult, followed by epileptogenesis, and ultimately ending in a state of recurrent, spontaneous seizures (epilepsy). The initial insult can take several forms and is followed by both rapid and slower progressive changes with rapid and slower durations. Rapid changes in animal models include neuronal excitation and calcium influx, triggering a cascade of events that include second messenger and immediate early gene responses, modifications to pre-existing proteins, and protein synthesis. Within days, there can be cell death and proliferation as well as inflammatory, glia, and vascular responses. Slower responses include growth (eg, axon outgrowth, synaptogenesis, angiogenesis), leading to synaptic reorganization, and this may in turn cause other changes. Over time, seizure threshold is lowered by a growing increase in excitability, and the risk of a seizure increases. These changes may be sufficient to cause epilepsy or may stall until a second "hit" occurs. The second hit could be environmental, or it could be due to time-dependent gene expression or co-morbidity. Therefore, genes, development, and the responses to the initial insult are likely to act together to result in a state of chronic seizures." (Scharfman, 2007) *Reproduced with permission from Springer Nature*.

This challenge in creating successful treatments suggests unknown mechanism that influence epilepsy. Whereas recent therapies have focused on neurons, glial cells and neuro-inflammation are rather understudied and might contribute to the disease phenotype (Choi and Koh, 2008; Vezzani et al., 2013). Understanding the underlying mechanisms behind epilepsy is necessary for the development of medicines and strategies to stop the progression of the disease.

1.1.1 Mechanisms underlying epilepsy

The exact mechanisms behind how seizures can initiate, and develop in the epileptic brain are not understood. Epilepsy is a complex disorder, and the development of epilepsy involves a multifaceted interplay of genetic factors, developmental disorder malformations as well as injuries to the brain. All of these factors lead to malfunctions in the inherent mechanisms that facilitate the regulation of neuronal firing (Scharfman, 2007).

There are numerous mechanisms to consider, but the main principle that is discussed is that seizures arise due to a disruption of mechanisms that normally create a balance between excitation and inhibition. Specifically that there is a disruption of the mechanisms that inhibit neuronal firing or a promotion of mechanisms that facilitate neuronal firing. Potential mechanisms include transmembrane gradients of neurons, as well synaptic transmission (Scharfman, 2007).

During epilepsy neurons become capable of repeated generation of action potentials (Khan et al., 2021). Normally, controls are in place to stop neurons from firing excessively. In a healthy brain, pumps such as the sodium potassium ATPase exist to maintain the chemical and electrical gradients of neurons. It pumps sodium extracellularly, and potassium intracellularly.

This keeps the neurons at a resting membrane potential of -60mV (McCormick and Huguenard, 1994).

Indeed, previous research has shown that the blockade of the sodium-potassium ATPase can lead to seizure activity (Vaillend et al., 2002). In addition, mutations in the subunits of voltage-dependent sodium channels can lead to epilepsy as well (Meisler et al., 2001). An abnormality such as activating of this channel at a more negative resting potential would allow an influx of sodium ions, leading to an increase in voltage across the neuronal membrane. As a result, the voltage of the neuronal membrane would approach the threshold voltage needed for neuronal depolarization, and would lower the threshold the neuron needs to cross in order to fire (Scharfman, 2007). All this together suggests that the disruption of the mechanisms involved with neuronal firing can lead to the development of epilepsy.

Separating out how exactly genetic factors, and environmental influences, such as injuries, lead to the development of epilepsy is difficult to do in human studies. This necessitates the use of animal models of epilepsy, so that the genetic and environmental factors and be better regulated.

1.2 Kainic acid as a model to study epilepsy

A large part of our understanding of epilepsy and its mechanisms comes from both human patients (including excised tissues and post-mortem studies) and models of epilepsy, primarily in rodents (Eyo et al., 2017). Studying epilepsy with animal models has many advantages; it allows for more control of the environment that the animals are raised in as well as their genetic background.

One of the most common ways to model epilepsy in mice and rats is by chemically inducing chronic seizures, specifically with kainic acid (KA) (Kandratavicius et al., 2014; Leite et al., 2002). This model mimics TLE, and has been shown to induce behavioral seizures and produce neuropathological lesions, such as neuronal degeneration in the CA3 region of the hippocampus, that are similar to what is seen in patients with TLE (Lévesque and Avoli, 2013). KA is a cyclic analog of L-glutamate and preferentially activates kainate glutamate receptor subtypes (Ben-Ari and Cossart, 2000). The injection of KA leads to hyper-synchronized excitatory neuronal activity, and induces *status epilepticus* (SE), which is a period of prolonged and recurrent seizures (Fisher et al., 2005), which eventually results in neuronal death (Lévesque and Avoli, 2013). Although the exact details of how seizures spread are not known, the hippocampus, and specifically CA1/CA3 region is recognized to be susceptible to KA. This is due to the high density of kainate receptors within this region, and makes the hippocampus the seizure onset zone in this model (Ben-Ari and Cossart, 2000; Lévesque and Avoli, 2013; Lisgaras and Scharfman, 2022). The consequence of SE is the production of pro-inflammatory

cytokines and chemokines, increased epileptiform spiking, neurodegeneration, excessive neurogenesis, reactive gliosis, and excessive production of reactive oxygen/nitrogen species (Sharma et al., 2019).

To determine the severity of seizures after KA injection, the Racine scale is used (Racine, 1972). This allows for seizure severity determination through behavioral readouts, without the need to record neuronal activity. The Racine scale divides the seizures into 5 stages: Stage-1: freezing behavior; Stage-2: rigid posture and tail; Stage-3: head nodding, rearing into a sitting position with forepaws shaking; Stage-4: rearing and occasional falling; Stage-5: bilateral forelimb clonus with rearing and loss of balance, repeated falling (Tse et al., 2014). Two types of spontaneous recurrent seizures have been identified; convulsive seizures (CS) and non-convulsive seizures (NCS). Stages 3-5 fall into the CS category and stages 1 and 2 fall into the NCS category (Puttachary et al., 2015; Tse et al., 2014).

1.2.2 EEG signal of seizures

Electroencephalography (EEG) is a method for measuring electrical signal of the entire brain, and represents the synchronous activity of global neuronal populations in the brain (Kim et al., 2024). It is a powerful tool for analyzing neural activity in both pathological and healthy conditions, and can be used to identify abrupt changes in neuronal activity as well as spiking patterns during abnormal neural discharges in response to external stimuli (Kyle et al., 2023). In epilepsy research, EEG signal is commonly used to define seizure occurrence, their frequency, and strength. Past studies have defined interictal spikes and seizures based on EEG spike characteristics such as, amplitude, inter-spike interval, duration, and power spectral analysis (Kyle et al., 2023).

One way to delve further into the EEG signal is to perform fast Fourier transforms (FFTs) to transform the temporal EEG data to the frequency domain from 0-100 Hz. This generates power bands that can be divided into separate ranges, including delta (0.5-4 Hz), beta (16-24 Hz) and gamma (24-80 Hz). The power of the different bands has been shown to change based on seizure state. One study showed that beta and especially gamma power peaked during stage 3 seizures, and declined in stage 4 and 5 before reaching baseline (Tse et al., 2014). The increase of power in the gamma power band has been found to be a reliable marker of seizure occurrence (Tito et al., 2009).

1.3 Microglia

Microglia are the resident macrophages of the central nervous system (CNS) (Eyo et al., 2014). They respond to environmental changes, including trauma, infections, inflammation, and pathologies (Nimmerjahn et al., 2005; Umpierre and Wu, 2021). Due to their motile

processes, microglia constitute a highly heterogeneous population of cells, exhibiting diverse morphologies depending on the signals they receive (**Figure 2**). They adapt their morphology as they surveille their local environment (Wake et al., 2009; Tremblay et al., 2010).

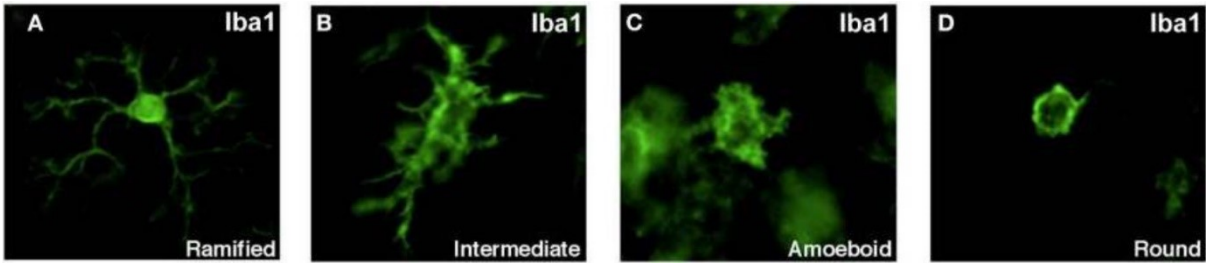

Figure 2: Distinct morphologies of Iba1+ microglia in adult rat brain; taken from: Ekdahl, C. T.

1.3.1 Role of microglia in health and disease

Microglia are integral cells of the central nervous system (CNS). They are highly dynamic motile cells that play an integral role in innate defense, and are involved in all CNS diseases (Kettenmann et al., 2013; Akiyoshi et al., 2018). They have been previously classified into two main states; resting/surveillant and activated to which they rapidly convert once they sense pathogenic signals (Kettenmann et al., 2013). Today, we know that microglia activation is a highly complex process, and it is has been shown to be more dynamic and diverse than previously described (Hanisch and Kettenmann, 2007; Augusto-Oliveira et al., 2022). Originally microglia were thought to be only resting cells that were waiting for pathological insults. This view changed when with *in vivo* 2-photon (2P) imaging in mice revealed that microglia processes are constantly extending and retracting in the intact healthy brain (Davalos et al., 2005; Nimmerjahn et al., 2005).

As microglia surveille their environment, they make contacts with neurons (Li et al., 2012; Tremblay et al., 2010; Wake et al., 2009), as well as modulate neurotransmission by modulating synaptic activity, and suppressing neuronal activity (Ji et al., 2013; Li et al., 2012; Paolicelli et al., 2011; Eyo et al., 2017).

Microglia are also crucial for learning and memory (Parkhurst et al., 2013), synaptic plasticity, and general cognitive function (Rogers et al., 2011; Sipe et al., 2016). During development, they prune synapses (Paolicelli et al., 2011; Schafer et al., 2013), regulate neurogenesis (Shigemoto-Mogami et al., 2014), promote neural precursor cell development (Cunningham et al., 2013), and help to clear apoptotic neurons (Sierra et al., 2010; Ahlers et al., 2015). All of these aspects show that microglia are relevant in the CNS physiological function as well as pathophysiological processes.

1.3.2 Microglia role in epilepsy

Even though the exact mechanism behind how microglia contribute to, and are involved with, epilepsy is not fully understood, there is evidence of microglia activation in epilepsy. Autopsy analysis of patients with intractable seizures revealed a 3- to 11-fold increase in microglial reactivity (Beach et al., 1995). Similarly, increased microglial immunoreactivity was observed in patients with focal cortical dysplasia known to trigger epilepsy (Boer et al., 2006). These findings indicate that microglia reactivity is a clinical feature of epilepsy.

Microglia roles in two parts of epilepsy: acute seizures, and the delayed neurodegeneration that occurs following seizures. This project focuses on microglia dynamics during acute seizures, in order to broaden our understanding of microglia responses to seizures and to help understand the underlying mechanisms controlling their interactions with neurons.

Real time *in vivo* descriptions of microglial dynamics during acute seizures, after an initial injury in the KA model of epilepsy are lacking, and the details underlying the mechanisms in which microglia interact with neurons under these conditions are not fully understood.

1.3.3 Microglia regulate neuronal activity

Although the regulation of neuronal activity in the brain has long been viewed as a function that is exclusive to neurons, recent studies have suggested a substantial contribution of microglia to this process (Li et al., 2012; Eyo et al., 2014; Akiyoshi et al., 2018; Wake et al., 2009; Feng et al., 2019; Cserép et al., 2020; Badimon et al., 2020). When excitable neurons recruit microglial processes, the neuronal activity is typically reduced following their interaction (Akiyoshi et al., 2018;Li et al., 2012). In addition, the ablation of microglia increases the susceptibility of mice to developing seizures after KA injection (Badimon et al., 2020).

Since seizures and epilepsy are based in abnormalities of neuronal function, and microglia are homeostatic regulators of the CNS, it stands to reason that microglia are involved in the regulation of neuronal activity (Hanisch and Kettenman, 2007; Tremblay et al., 2011).

Microglia exhibit enhanced process motility in conditions where local or global neuronal activity increases (Umpierre and Wu, 2021). While microglia have been shown to make contacts with neurons seemingly at random (Davalos et al., 2005; Nimmerjahn et al., 2005), they have recently been shown to extend processes towards active neurons (Akiyoshi et al., 2018; Eyo et al., 2014; Li et al., 2012). This process extension seems to be mediated by neuronal ATP/ADP release, acting on microglial P2Y12 receptors (Haynes et al.,2006; Badimon et al., 2020). Most of the recent evidence suggests that microglial responses to neuronal hyperactivity promotes homeostasis, and that microglial interaction with neurons reduces neuronal firing and dampens seizure (Akiyoshi et al., 2018; Badimon et al., 2020; Eyo et al., 2016; Eyo et al., 2014; Li et al., 2012; Merlini et al., 2021).

1.4 Microglia tracking

Changes in microglia motility are theorized to be a critical first step in their response to environmental changes, and analyzing microglial morphology can give us information about how the microglia are responding to their environment and about their function (Umpierre and Wu, 2021; Colombo et al., 2022).

Microglia motility is a broad term and can be divided into two main categories; (1) whole cell metrics and (2) subcellular metrics. (1) refers to metrics such as whole cell volume or surface area to analyze motility changes of a whole microglia, while (2) involves movement at the level of individual processes such as speed, length, and number of processes (Kyrargyri et al., 2019). My thesis aimed to focus on whole cell metrics, with the ultimate objective of potentially being able to study subcellular metrics.

1.4.1 2-Photon *in vivo* imaging for accurate microglia morphological analysis

Two-photon imaging (2P) is a fluorescence-based laser scanning microscopy technique. It involves two infrared photons that simultaneously excite a single fluorophore in a sample, which causes it to emit light at a specific wavelength. Compared to confocal microscopy, it has many advantages, including reduced damage to tissues, and greater penetration of up to 2 mm in the brain. It has similarities to confocal imaging, such as optical slicing capabilities, the ability to create 3-dimensional (3D) visualizations, as well as a high subcellular resolution of about 400 nanometers (Helmchen and Winfried, 2005; Douma et al., 2007)

2P can be used to study changes in microglial morphology (ramification), and process dynamics (surveillance and directed motility) (Kyrargyri et al., 2019).

Our goal was to refine *in vivo* imaging parameters to accurately track subcellular microglia dynamics. Defining these parameters involved two main factors: speed and resolution. To accurately track individual microglial processes, a high spatial resolution is needed in x, y, and z axis. The imaging also needs a high temporal resolution, so that the movement of the microglial processes is recorded as much as possible. Microglia have been shown to have distinct structural dynamics over tens of seconds (Davalos et al., 2005).

1.5 Aims of this thesis

While previous research hints at microglial involvement in controlling neuronal firing, the exact relationship between microglia and seizure progression in epilepsy remains unclear. Most studies have examine microglia dynamics in *ex vivo* settings, as well as long-term activation of microglia in response to seizure initiation, overlooking their response to acute seizures. The integration of 2P miscroscopy and EEG signal recording could help directly correlate microglia dynamic changes to the EEG signal during different stages of seizure activity.

Therefore, the following aims were outlined:

1. Determine the appropriate dosage of KA for inducing seizures in mice to be used during *in vivo* imaging.

2. Refine the methodologies for *in vivo* two-photon imaging to accurately track microglial dynamics in response to seizure activity.

3. Combine two-photon microscopy with electroencephalogram (EEG) recording technique in a single experimental setup, enabling simultaneous monitoring of microglial dynamics and seizure activity in awake mouse.

4. Utilize the optimized methodologies to investigate acute microglial responses to seizure activity in the KA-induced epilepsy model, focusing on the dynamic changes in microglial morphology and motility during and following seizure events.

By addressing these aims, this thesis endeavors to deepen our understanding of the role microglia play in epilepsy, and seizures.

2. Materials and methods

2.1 Animal handling

2.1.1 Housing

Animals were kept according to the TVG 2012 for the use of laboratory animals in experiments law with the project number 2021-0.607.460. Mice were housed in individually ventilated cages with a day and night cycle of 12 hours light and 12 hours dark. They received a standard diet (Altr. 1324 maintenance diet or Altr. 1314 breeding diet, Altromin Spezialfutter GmbH&Co.KG).

2.1.2 Mouse strains

The mouse strains were purchased from Jackson Laboratory and are bred in house in the preclinical facility of ISTA (Am Campus 1, 3400 Klosterneuburg).

C57BL/6J (Black 6)

The C57BL/6J mice are the most widely used inbred strain for research. This strain was used as the wildtype (WT) mice in this project (The Jackson Laboratory, C57BL/6J).

CX_3CR1^{GFP}

CX_3CR1^{GFP} mice express enhanced green fluorescent protein (EGFP) in monocytes, dendritic cells, NK, cells and brain microglia under the control of the endogenous Cx3cr1 locus)(The Jackson Laboratory, CX_3CR1^{GFP}). The mice used were heterozygous, as the homozygous mice in this strain have microglia whose functions are impaired (Cardona et al., 2006).

2.2 Kainic acid model

2.2.1 Kainic acid preparation

10 mg of Kainic acid (KA) (Sigma-Aldrich, K0250-10MG) was resolved and diluted from its powder form and suspended by adding 1000 µL MilliQ water to the KA. This solution was then vortexed for 3 minutes, sonicated for 10 minutes at 30ºC, vortexed again for 1 minute, and sonicated for 20 minutes at 40ºC. Then additional 4 mL of MilliQ was added, in order to achieve the target dilution of 2 mg/mL. The solution was then vortexed for another 3 minutes. The resolved KA were aliquoted and stored at -80ºC for up to 6 months.

2.2.2 KA injection

For the initial experiments to determine the KA dosage, the mice were restrained in a head down position and *intraperitoneal* (*i.p.*) injected with the KA dosage with a 26-gauge needle (Henry Schein Medical) in the abdomen with the needle entering at a 45º angle.

For the *in vivo* imaging experiments, the mice were briefly anesthetized with isoflurane (Zoetis) while still head-fixed. Animals were gently lifted by the tail, and *i.p.* injected.

2.2.3 Seizure severity determination

Seizure severity determination was done between 1 pm and 3 pm to avoid variations due to the circadian rhythms of the mice. After KA injection, the mice were each placed back inside their cage and observed for the state of their behavior over 2 hours every 5 minutes using the Racine scale (Tse et al., 2014; Racine 1972). Stage-1: freezing behavior; Stage-2: rigid posture and tail; Stage-3 head nodding, rearing into a sitting position with forepaws shaking; Stage-4: rearing and occasional falling; Stage-5: bilateral forelimb clonus with rearing and loss of balance, repeated falling. The mice were sacrificed about 2 hours after the KA injection, and perfused with 1X Phosphate-buffered saline (PBS) + 0.01% (w/v) Heparin and then 4% (w/v) paraformaldehyde (PFA)/ PBS. The brains were kept in 4% PFA for 24hrs, and then transferred to PBS and stored at 4ºC until used for histology.

2.3 EEG and cranial window

2.3.1 Electrode build

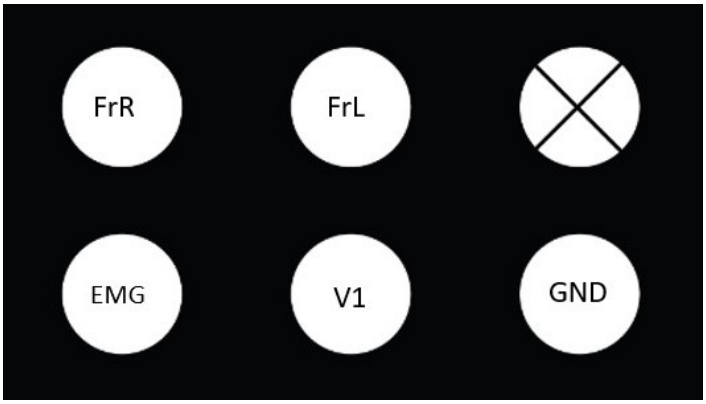

Figure 3: Millmax schematic, pin labels shown in circles. FrL: frontal left lobe, FrR: frontal right lobe, V1: visual cortex. EMG: Electromyography, GND: ground.

First, we took the insulated wire and folded it in half. We then twisted it until it was tightly wound. We then measured and cut the twisted wire into five pieces: one piece measuring 3 cm, two pieces measuring 2 cm each, and two pieces measuring 1 cm each. Following this, we took a drop of solder and carefully de-insulated the ends of the five pieces of wire. With

the ends expose, we soldered each wire to its designated pin: the 3 cm wire to the EMG pin of the milmax, the 2 cm wires to FrL and FrR, and the 1 cm wires to the V1 and GND pins (as shown in Figure 3). Then we obtained four Microdrive Gold Pins and removed the lower thin ends from each one. We soldered these gold pin ends onto the end of each wire, except for the 3 cm EMG one, ensuring that the wire was attached about halfway down the pin. We measured the length from the round end of each pin to its wire, making sure that the length fell between 0.7 and 0.9 mm. After each pin was soldered, the cut end was cut again as close to the attached wire as possible. For the 3 cm EMG wire, we soldered the unused larger end of one of the Microdrive Gold Pins, attaching the wire to the cut end. Finally, we placed the completed electrode into a petri dish and disinfected with 70% (v/v) ETOH in distilled water, and 1 hour of UV light.

2.3.2 Anesthesia and surgical preparation

CX_3CR1^{GFP} mice were anesthetized with isoflurane (5% (v/v) induction, 2.5% (v/v) maintenance) in 0.6 L/min O_2 and were kept at 37ºC using a heating pad connected to a rectal probe during the surgical procedure. The mouse was then placed in a stereotaxic frame (KOPF digital plus). The depth of anesthesia was observed by monitoring the breathing rate. To prevent corneal dehydration, eye ointment (Oleo Vital) was applied. The head was shaved and disinfected with 70% (v/v) ETOH in distilled water, and an incision in the scalp was made, and a flap of skin was removed covering both hemispheres. A scalpel was used to cut two small muscles connected to the back of the skull in order to create more surface area for the glue to adhere to, and to reveal the back of the skull where the GND electrode will be placed. To make space for the EMG electrode the fat at the back of the head by the neck, was removed using a scalpel. Then, a curved forceps was placed in the space between the exposed muscle and the skin and opened. Finally, the skull was cleaned with a 3% (v/v) solution of hydrogen peroxide (Sigma, Cat#216763) in PBS.

2.3.3 Cranial Window Surgery

After the surgical preparation, a 3 mm biopsy tool (Henry Schein) was used to mark the skull for drilling, placed on the right hemisphere next to the midline at the posterior part of the skull, above the primary visual cortex. After this, the craniotomy was gently performed with a micro drill. A double glass window made of 3- and 5-mm glass coverslips (Multi Channel Systems), which had been joined together with an ultraviolet curable adhesive, was adhered to the skull using a mixture of dental cement powder (Henry Schein) and super glue.

2.3.4 EEG Implantation

Brain region:	Bregma:	Interaural
FrR	2.5 mm	1.5 mm
FrL	2.5 mm	-1.5 mm
V1	-3 mm	1.65 mm

Table 1: List of coordinates used to implant electrodes. FrL: frontal left lobe, FrR: frontal right lobe, V1: visual cortex.

After the window placement, the electrodes were implanted. First, the coordinates were marked (**Table 1**), and a mark was made with a water-resistant marker. Then, the holes for the electrodes were drilled at the marks using a 0.9 mm drill bit starting with the FrR pin. After the hole was drilled, the pin was gently placed into the hole, and a drop of dental cement was placed onto the pin. The next hole and pin placement were performed after the previous drop of cement hardened, to avoid the pin moving and losing contact with the brain surface. The next pin placements followed in this order: FrL, V1, and GND, making sure that the millmax was correctly oriented with the GND at the bottom left. Finally, the EMG electrode was placed in the pocket created between the muscle and skin at the back left side of the neck. The skin above the EMG placement at the base of the skull was sutured together. All the wires were gently bent into place such that they were flat to the skull, and not blocking the window, the millmax was also gently positioned so that it was closer to the back of the head, but angled in a way that the area around the window was not be blocked. Dental cement was then placed around the cranial window, and a custom-built head-plate was placed onto it. Next, the rest of the skull and the sides of the head-plate as well as the exposed wires and pins attached to the millmax were covered. Layers of cement were added around the base of the millmax until all of the wire and pins were protected.

The post-surgery analgesia management was controlled with Metamizol (Sanofi Aventis, Cat#Ay005, 200 mg/kg during surgery) and with Meloxicam (Boehringer-Ingelheim, Cat#KPOEH3R, *s.c.* 5 mg/kg after surgery every 24 h for 3 consecutive days). The animals were left to recover for at least 2 weeks before being used for experiments.

2.4 Two-photon imaging and EEG recording

2.4.1 Image acquisition

2-Photon image acquisition

Cx3cr1eGFP/+ mice (8-10 weeks) were imaged using a Leica TCS SP8 DIVE CS microscope, equipped with a 25 x/0.95 W water immersion objective (HC Fuotar WD=2.5 mm, wide angle (41º)) with laser tuned to 920 nm. A zoom of 1.5x was used to acquire a 295.26 x 295.26 µm

field of view of 1504 x 1504 pixels. A z-stack size of 68.96 µm, with 47 z-steps of size 1.5 µm was acquired. Each z-stack was imaged in 1 min and 53 seconds, continuously. The imaging started with a 10-minute baseline, followed by about 2 hours of imaging. The 2-hour imaging window was separated into four acquisition windows, each about 30 minutes long. After each acquisition window, the drift was visually corrected to the first frame of the baseline recording.

The images were processed in Imaris v9.9.1, using a median filter, background subtraction and normalized over z. The videos were drift corrected using the Imaris Spot function, with a spot size set to 7 µm, and automatic spot creation.

Confocal image acquisition

The CA3 and DG brain areas were imaged to confirm previous results suggesting increased microglial reactivity. 16-bit confocal images were acquired with a Zeiss LSM900 microscope equipped with a 40 x Plan-Apochromat oil objective (40 x/1.3 Oil DIC, UV-IR WD=0.2). A 303.85 x 303.85 µm field of view was imaged with 1948 x 1948 pixels, giving 0.155 µm/pixel in XY and a Z-step size of 0.26 µm.

Images were stitched using the Imaris Stitcher v9.9.1 software and were Gaussian filtered, background subtracted, and normalized over z in Imaris v9.9.1.

2.4.2 EEG recording

In order to record our EEG signal we first connected the RHD ultra-thin SPI interface cable to the RHD USB interface board. We then connected the RHD USB board to the laptop with a USB cable. The printed circuit adapter is connected to the RHD/RHS head-stage with the 16-channel Onetics adapter that was already soldered to the printed circuit adapter. After all of this was set up, the mouse was placed inside the Faraday cage and head-fixed. To connect the electrode to the adapter, we soldered the printed circuit adapter to a milmax 2X19-Pin male-male, and attached it to a milmax 2X19-Pin male-female. We attached this milmax to the electrode's milmax at the back of the mouse's head, making sure that the orientation was correct, and that the ground was at the bottom left. Once everything was connected, we opened the acquisition software (Intan RHX Data Acquisition software version 3.0.2) and set the sampling rate to 20 kHz.

2.4.3 EEG recording analysis

Preprocessing:

As we intend to analyze frequencies up to 400Hz, we down sampled the EEG raw signal to 1KHz (initially 20KHz) to make the signal processing analysis pipeline faster. After down sampling, the signal is notch filtered (50Hz, and its harmonics which are 100Hz, 150Hz) to

remove the power line noise and band pass filtered from 1Hz to 400Hz. In the next step, we re-referenced the signal to the average of the channels. In this way, we are able to detect the noise which had been picked up by all the channels, and which was then removed from the signal.

Fourier domain analysis:

We used FFT (Fast Fourier Transform) to calculate the DFT (Discrete Fourier Transform) of the signal. As we want to track the power of different frequency bands over time, we used STFT (Short Time Fourier Transform) to calculate the power of frequency components over time. We used a two seconds Hanning window with an overlap of one second between every two sequential windows.

2.5 Immunohistochemistry

2.5.1 Solution formulation

Buffer	**Formulation**
4% (w/v) Paraformaldehyde (PFA)	1XPBS, Paraformaldehyde, pH=6.9
Antifade	Mowidol 4-88 reagent, Glycerol, 0.2 M Tris buffer pH 8, sterile water, 1,4 Diazabicyclo-octane
Solutions for staining:	
Blocking solution	1% (w/v) BSA, 1X PBS, 0.5% (v/v) Na Azide, 10% (v/v) Serum (goat), 5% (v/v) Triton 100, ddH_2O
Antibody solution	1% (w/v) BSA, 1X PBS, 0.5% (v/v) Na Azide, 3% (v/v) Serum (goat), 5% (v/v) Triton 100, ddH_2O

Table 3: List of solutions used for immunohistochemistry

Antibody	**Dilution**	**Company**
Primary antibody		
Anti Iba1 rabbit	1:750	Gene Tex
Anti CD68 rat	1:250	Bio-Rad
Secondary antibody		
Goat anti rabbit 568	1:2000	Thermo Fisher Scientific
Goat anti rat 647	1:2000	Thermo Fisher Scientific

Table 2: List of primary and secondary antibodies used

2.5.2 Dissection

Mice were briefly anesthetized with isoflurane and then transcardially perfused with 1X PBS + 0.01% (w/v) Heparin, and then with 4% (w/v) PFA/PBS. After perfusion, the mouse was decapitated and the brain was dissected out from the skull, placed into a falcon tube with 4% PFA (w/v) in PBS, post-fixed for 24 hrs at 4ºC, and then transferred and stored in 1X PBS at 4ºC.

2.5.3 Slicing with vibratom

Brains were sliced with a Leica VT 1200S Vibratom. 100 mL of 3% agarose (w/v) in PBS was prepared and heated up in the microwave for 1 min and 30 sec. The agarose gel was placed in a 6 well-plate after cooling to 60ºC. The brain was then placed in the agarose, and then covered fully with the left over agarose. After cooling down, the agarose surrounding the brain was cut close to the size of the brain. The block of agarose was then superglued onto a Leica VT 1200S Vibratom stage, which was then filled with 1X PBS. The brain was sliced at a speed of 0.6 mm/s and a thickness of 100 µm. The brain slices were placed in 1X PBS in a 12-well plate.

2.5.4 Immunostaining of brain slices

Brain slices were placed in 30% (w/v) Sucrose/PBS solution. After the slices sunk to the bottom of the well plate, the plate was placed on dry ice until the sucrose and slices were frozen. They were then placed at RT until thawed. This was done two more times. Slices were washed with 1X PBS for 10 minutes and then incubated with 1000µL of goat blocking solution (**Table 2**) for 1 hour at RT on a shaker. Next, they were incubated with 1000µL antibody solution containing the primary antibodies (**Table 3**) for at least 2 days at 4ºC.

The slices were washed three times with 1X PBS for 30 minutes. Then they were incubated with 1000 µL of antibody solution containing the secondary antibodies (**Table 3**) for 2 hours at RT. Afterwards, the slices were washed three times with 1X PBS for 30 minutes. Finally, the slices were incubated with Hoechst 33342 (1:5000) in 1X PBS for 10 minutes. The slices were mounted on a glass microscope slide (Assistant, Cat#42406020) with a paintbrush. The remaining PBS was removed with a Kimtech wipe, and 158µL of Antifade solution (**Table 2**) was pipetted onto the slide. Finally, a coverslip (Menzel-Glaser #0) was placed.

2.6 Image processing and analysis

2.6.1 CD68 volume analysis:

The percent volume of CD68 inside microglia was analyzed using the Imaris v9.9.1 surface function. The CD68 surfaces were created with Surface detail of 0.312 µm, and a background

subtraction with diameter of largest sphere of 1.17 µm. The microglia surfaces were created using Surface detail of 0.312 µm, and a background subtraction with diameter of largest sphere of 1.17 µm. They were then filtered to exclude area's below 10 μm^2. The surface-surface coloc MatLab plug-in was then used to find the amount of CD68 volume within the microglia volume. The volume statistics of the co-localized surface was exported as well as the microglia volume as csv files.

2.6.2 Microglia volume

First, the videos were cropped so that any cells that drifted in or out-of-view were cropped out. The videos were normalized over time using the normalize time points MatLab plugin. The Imaris surface function was used to find the volume of the cells, with surface detail set to 0.5 µm and smoothing to 1.0 µm. Then the surface volume statistics were exported as csv files.

2.6.3 Process tracking

The image processing was done in Imaris v9.9.1, and then imported to ImageJ 2.9.0/1.53t. This was done by adapting the method described in Eyo et al., 2014. A few processes were tracked using the Manual tracking plugin. The track data was then saved and imported to Python 3.11 and graphs were plotted there.

2.7 Quantification

CD68 quantification

The percent of the co-localized surface inside the microglia volume was found for each dosage for the V1. This was then normalized to the control. A one-way ANOVA was done between all the different dosages. Significance was defined with a P-value <0.05. None of them were significant. The control had an n of 1, and the other dosages had an n of 3. Each n is one mouse with one image.

Microglia volume and EEG signal correlation

The filtered EEG signal was loaded into Python 3.11. The end of the EEG signal was shortened so that it had the same length in time as the imaging window. This signal was then separated into bins. This number was equal to the number of z-stacks of frames acquired by the 2-photon microscope. The mean of the overall EEG power for each bin was calculated.

The microglia surface volumes were summed in Python. This number was then correlated to the mean EEG power via Pearson's correlation.

3. Results

Part 1

3.1 Determining KA concentration for *in vivo* imaging

The first step of this project was to identify the correct dosage of kainic acid (KA) for eliciting the desired seizure stages 1 and 2, which would describe a mild seizure behavioral response that would allow simultaneously *in vivo* imaging of microglia dynamics at later stages.

Stage 3, 4, and 5 are convulsive seizures, and have an obvious behavioral readout, while stage 1 and 2 are non-convulsive seizures, and have a more subtle behavioral readout. Stage 4 and 5 are more severe than stage 3, and involve the mouse falling over repeatedly and eventually jumping around wildly (**Figure 4b**). As the goal for this project was to image head-fixed mice, and look at how microglia respond to seizure activity, stage 4 and 5 were determined to be too severe. There is a chance that the mouse would move too much, which could affect the imaging data as well as the EEG data. The range of motion of the mice would be restricted, and we wanted to avoid the possibility that the mice could injure themselves while convulsing.

To determine the ideal KA dosage, we injected mice with varying levels of KA. We injected the mice via *intraperitoneal* (*i.p.*) route, and then observed their behavior over two hours, noting the seizure stage every 5 minutes (**Figure 4a**). At the lowest dose of 10 mg/kg two of the three mice reached stage 2, while the other mouse only reached stage 1. At 20 mg/kg all mice reached stage 2, but only one of the three mice reached stage 3-5. Finally at 30 mg/kg all mice reached stage 5, and one of the three mice died during the observation (this mouse was excluded from the data analysis) (**Figure 4c**). Based on these results, we decided that 30 mg/kg was too high of a dose and would result in too severe of a seizure phenotype, and a high likelihood of death. The lowest dose of 10 mg/kg was too low, as two out of the three mice injected only reached stage 1. To conclude, the ideal dose was determined to be 20 mg/kg in order to have a higher chance of reaching the ideal seizure stage for *in vivo* imaging.

b

Representative illustration:					
Stage:	1	2	3	4	5
Stage criteria:	Absence-like immobility	Hunching with facial automatism	Rearing with facial automatism and forelimb clonus	Repeated rearing with continuous forelimb clonus and falling (loss of righting reflex)	Generalized tonic–clonic convulsions with lateral recumbence or jumping and wild running followed by generalized convulsions

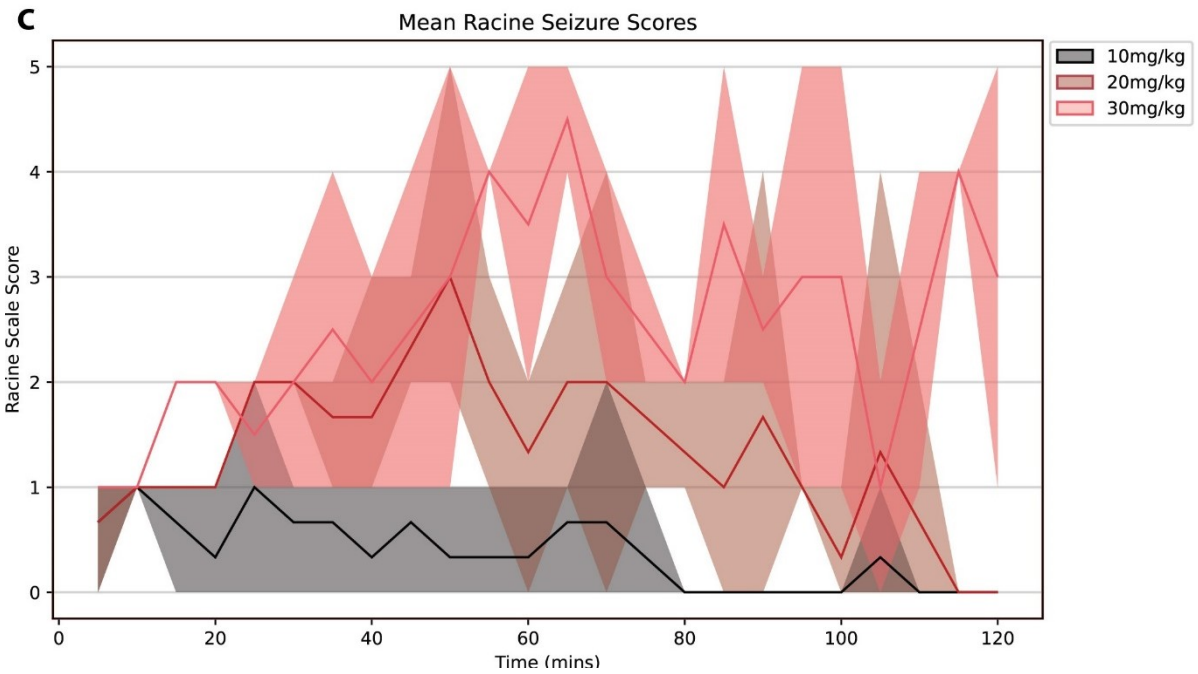

Figure 4: Racine seizure monitoring. a. Schematic of the behavioral monitoring timeline after kainic acid (KA) injection. **b.** Table showing representative images of seizure stages and the criteria used to determine seizure stage (Tse et al., 2014). **c.** Graph showing the Racine seizure score across 3 different KA concentrations over 2 hours. Seizure stages were scored every 5 minutes. Lines show mean seizure scores between all mice in each dosage, and the shading represents the entire range of seizure scores of all mice within each dosage.

3.2 Identify microglia reactivity

After identifying the optimal KA dosage, the next step was to determine if microglia morphological and molecular activation occurs in the mouse 2 hours after the initial KA injection, and specifically in the primary visual cortex (V1) of the mice. Previous studies had determined microglial reactivity in the CA3 and CA1 regions of the hippocampus (Beach et al., 1995; Avignone et al., 2008; Rappold et al., 2006; Eyo et al., 2014), and acute microglial response in the cortex, more specifically the V1, needed to be confirmed.

3.2.1 Microglia have increased ramification and reactive appearance 2 hrs after KA injection

To confirm previous published results indicating acute microglial reactivity after KA injection (Eyo et al., 2014; Umpierre et al., 2020), the mice were sacrificed 2 hrs after KA injection (**Figure 4a**). We focused on the DG and the CA3 regions, as they are areas that have been shown to be involved in seizure propagation during SE, as well as areas of increased neuronal death (Lévesque and Avoli, 2013).

As seen in **Figure 5**, no obvious morphological changes of the microglia can be observed when comparing the 10 mg/kg dose (second column) to the control (first column) across all three brain areas. In the DG and the CA3 regions, noticeable changes are evident at the 20 mg/kg dosage (**Figure 5a, b**). Microglia exhibit a clear alteration in morphology. This persists at the 30 mg/kg dose. Conversely, in the V1, the microglia do not exhibit apparent morphological changes at the 10 and 20 mg/kg doses (**Figure 5c**). However, at the 30 mg/kg dose, they adopt a more hyper-ramified state, which includes an increase in process branching, and an increase in process numbers. In summary, we were able to confirm the microglial reactivity 2 h after KA injection in the DG and the CA3 at the 20 and 30 mg/kg dose, and in the V1 at the 30 mg/kg dose.

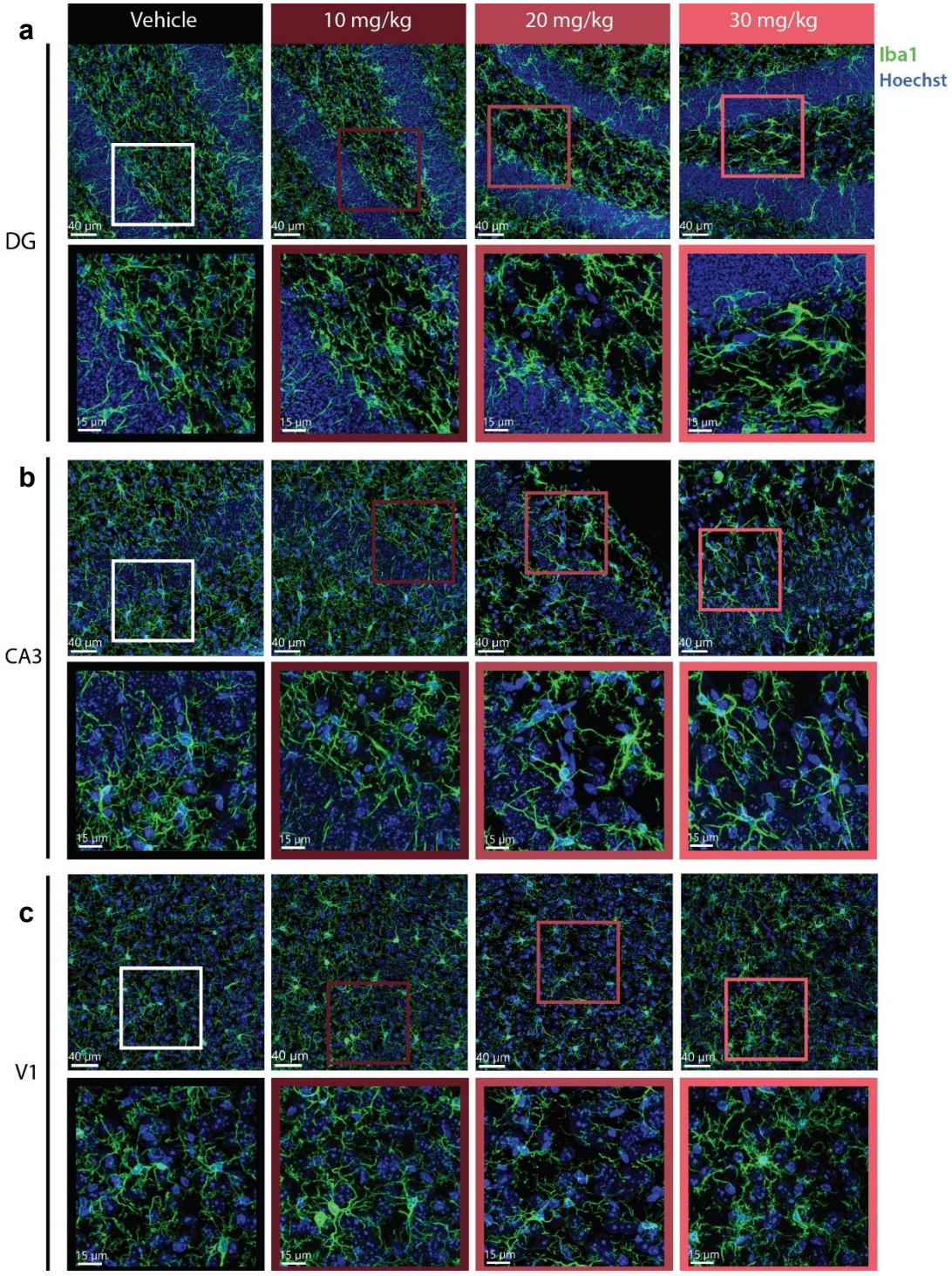

Figure 5: Microglia morphology adapts upon different KA dosages. Representative confocal images of microglia across 3 different brain areas; **a.** the dentate gyrus (DG), **b.** the hippocampal CA3 region, and **c.** the primary visual cortex (V1). Shows 4 different conditions: Vehicle (MilliQ water), 10 mg/kg, 20 mg/kg and 30 mg/kg KA doses. Overview: 40 µm, zoomed in: 15 µm.

3.2.2 CD68 volume percentage

To further characterize microglial reactivity V1 at varying doses of KA, we performed immunohistochemical staining for CD68. CD68 was chosen as it is a lysosomal marker that is typically upregulated during inflammation by activated microglia/macrophages (Jurga et al., 2020; Broekaart et al., 2018).

The CD68 volume was quantified by measuring the percent volume inside the microglia. The CD68 expression increased at the 10 mg/kg dose when compared to the control, as well as at the 20 mg dose. The elevation of CD68 expression at the 10 mg/kg dose is even more pronounced compared to both the 20 mg/kg and 30 mg/kg dose (**Figure 6a**). This increase in CD68 expression was reflected in the quantification of the CD68 volume. At the 10 mg/kg dose, a wide range was observed, with the mean exceeding that of both the 20 mg/kg and 30 mg/kg mean percent of CD68 within the microglia (**Figure 6b**). The expression of the CD68 marker is comparable between the 30 mg/kg and the control, not much difference can be seen.

Overall, we observed an increase in CD68 expression in the V1 of mice injected with KA compared to the control, though this increase did not correlate with increasing KA dosage.

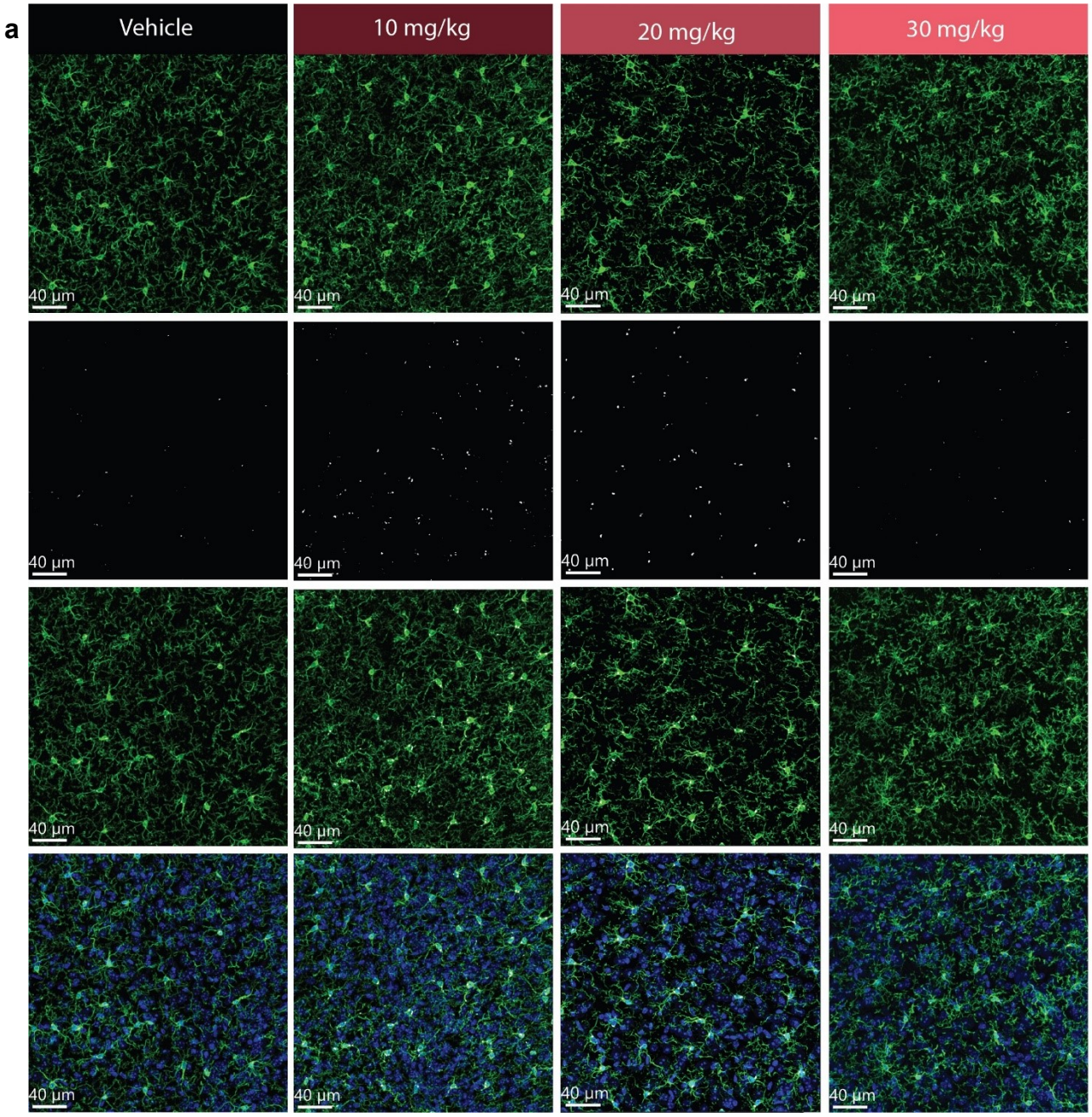

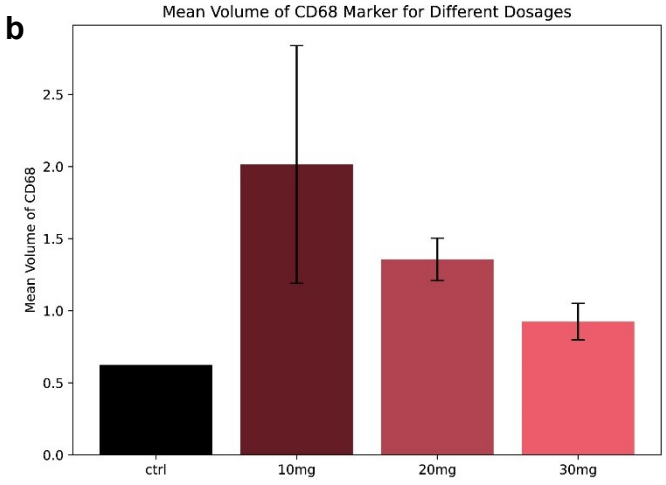

Figure 6 : CD68 volume changes with differences in KA dose. **a.** Representative confocal images from a C57BL/6J following either vehicle injection (left column) or kainic acid (KA) injection. Iba1 (green, microglia), CD68 (white), the nuclei-dye Hoechst (blue). Scale bar 40 µm. **b.** Percent of total CD68 volume within microglia volume normalized to control. Not significant between all doses. (n = 1 for control, and 3 for the doses.)

PART 2

3.3 Optimizing *in vivo* imaging for detailed microglia tracking

Next we implemented the 2-photon (2P) imaging method The end goal for the 2P parameters optimization was to be able to track microglia subcellular structures, and to be able to distinguish the individual process arms and their ends.

3.3.1 Imaging parameter optimization

To define the correct metrics for imaging, CX3CR1$^{GFP/+}$ mice (Jung et al., 2000) were used. We performed the cranial window surgery, and then left the mice to recover for 2-3 weeks to mitigate microglia activation from the surgery. This was followed by 3 days of habituation to reduce the stress the mice would experience during imaging (**Figure 7a**). The initial testing was done with a 16X objective, to image as many cells as possible. The z-stack size of 189.99 µm, with a 2.5 µm z-step size. One z-stack took 1 min and 56 sec (**Figure 7d**). This initial test showed that a large z-stack could be obtained under 2 minutes, but the end result showed that the image would not be usable for the wanted outcome. The signal to noise ratio was not high enough to allow for precise tracking of microglia dynamics. Even after image processing of experiment 1, the individual microglia were blurry, and without defined processes (**Figure 7c**). The second significant change in imaging parameters included the use of a 26X water immersion objective, in order to increase the resolution. Additionally, we reduced the z-stack size to 85.45 µm, and adjusted the z-step size of 1.5 µm, aiming to capture finer details along the z-axis. This modification not only improved the z-axis resolution but also facilitated faster acquisition. This allowed for a higher resolution image to be acquired within 2 minutes (**Figure 7d**). While the image quality markedly improved, pinpointing individual microglia processes remained difficult to identify and could pose potential issues for accurate tracking (**Figure 7c**).

For the third major step in image parameter optimization, both the z-stack size and the z-step size were reduced, while the speed of acquisition was decreased to 400 Hz, to increase the signal-to-noise ratio. We also zoomed in further to 1.5X, which increases the detail, and allows for the same number of pixels to be imaged but over a smaller area (**Figure 7d**). The resulting image allowed for individual microglia process identification as well as a good signal-to-noise ratio. Test tracking of processes revealed that with this level of image quality, we were able to track processes (**Figure 8a**).

For the final step in parameter optimization, we utilized the Leica Dive microscope Lightning Mode (experiment 4, **Figure 7d**). This is a mode that deconvolutes the images taken at the microscope. It enables a higher resolution image to be acquired, and lead us to be able to image a z-stack at a faster speed, and a higher resolution. The resolution for experiment 4 with the Lightning mode was 1552x1552, with a speed of 672 Hz. The z-stack was slightly reduced to 68.96 µm, with a z-step size of 1.5 µm and was imaged in 1 min and 53 seconds. Additionally, z-compensation was implemented, and the laser power was adjusted

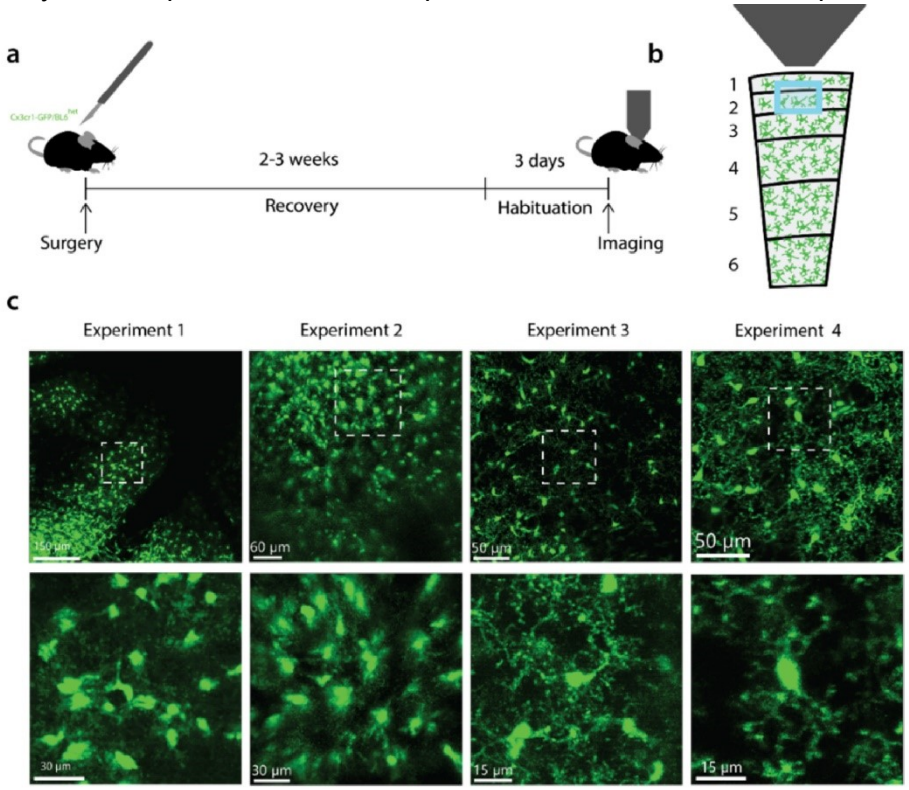

d

Parameters	Experiment 1	Experiment 2	Experiment 3	Experiment 4
objective:	16X	26X	26X	26X
resolution:	1024x1024	1024x1024	1024x1024	1552x1552
speed:	400 Hz	600 Hz	400 Hz	672 Hz
z-stack size:	189.99 µm	85.45 µm	75.05 µm	68.96 µm
z step size:	2.5 µm	1.5 µm	1 µm	1.5 µm
z-stack time:	1min 56sec	1min 45sec	1min 46sec	1min 53sec
num. z steps:	77	57	76	47
laser power:	15	13	8	10->15
zoom:	1.5	1	1.5	2.25
bidirectional:	yes	yes	yes	yes
line Avg:	no	2	2	2
LNG:	no	no	no	yes

Figure 7: Parameter optimization for *in vivo* imaging. **a**. Schematic of timeline from surgery to imaging. **b**. Schematic of imaging depth in the V1. **c**. Images of different stages of imaging acquisition (from left to right): 150 µm, 60 µm, 50 µm, 50 µm (top); 30 µm, 30 µm, 15 µm, 15 µm (bottom). **d**. Table showing the parameters that were changed to improve the image quality at the 2-photon microscope. Lightning mode (LNG)

incrementally from 10 to 15 mW, gradually increasing from the top to the deeper layers of the z-stack (**Figure 7d**). This optimization ensured a more even fluorescence throughout the z-stack. This final step allowed for high signal-to-noise ratio, and for the end of the process arms to be visually identified (**Figure 8a'**).

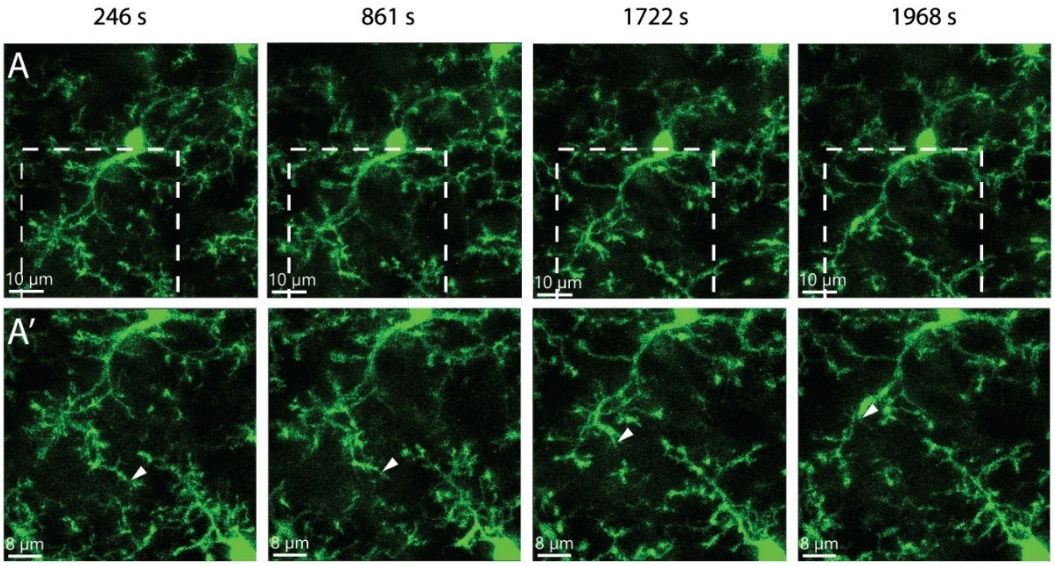

Figure 8: Microglia process retracting over time. a. A microglia cell over 4 different time frames. Scale bar 10 µm **a'.** Zoomed in view of microglia in (**a**), white arrow follows a process end retracting. Scale bar 8 µm. Microglia in green.

3.3.2 Tracking microglia fine processes

After the imaging parameters were set up, the next step was to try different methods of tracking microglia processes. This would not have been possible using the metrics in experiments 1, and 2 (**Figure 7c**), as these images had a low signal-to-noise ratio, and individual processes could not be identified. Tracking microglia processes requires a high resolution to precisely track motility. Key tracking parameters include the xyz position and the velocity of the processes.

Many different approaches have been developed to evaluate microglial process motility, such as volume/area occupied by microglia processes (Davalos et al., 2005), microglia volume, area, number of branches per cell (Eyo et al., 2016; Eyo et al., 2014; Abiega et al., 2016) and process length or speed (Feng et al., 2019; Avignone et al., 2015; Nimmerjahn et al., 2005). We decided to first focus on microglia process speed and position, as this is a direct measurement in process motility. The position and movement of microglia processes is a parameter that reflects how they are scanning their environment, and responding to external cues. Previous studies have shown changes in process dynamics in response to KA injection,

including an increase in elongation velocity, and an increase in area explored (Avignone et al., 2015).

Figure 9a-c shows the result of the 2D tracking that was implemented using the Manual tracking plugin in Image J. The process end velocity and distance was able to be plotted over time. Finally, the spot function in Imaris was used to manually track the ends of processes in a cell from experiment 4 in **Figure 9d-f**. We were able to manually track the process ends over time, in 3D.

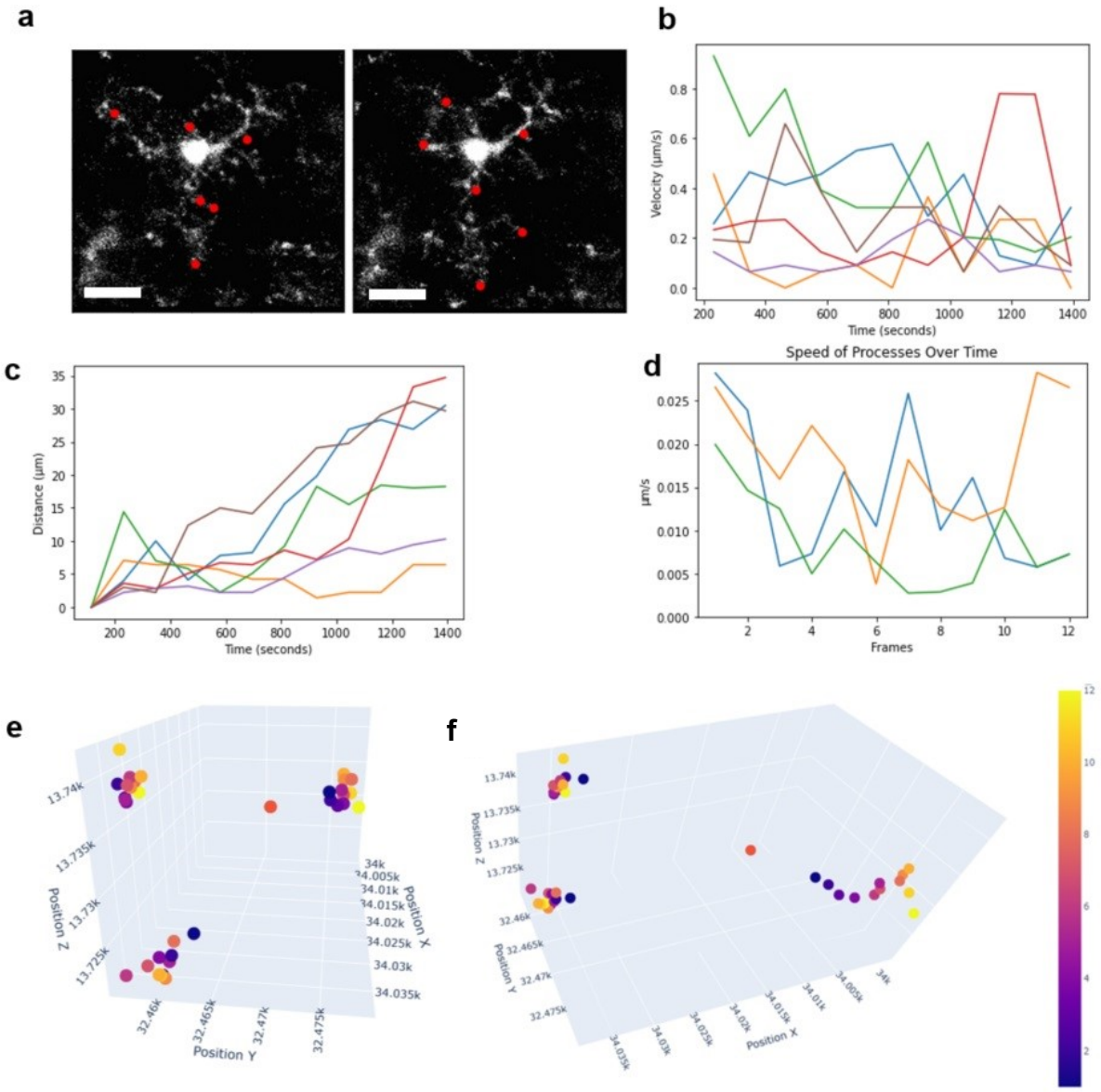

Figure 9: Initial tracking of microglial processes. a. A maximum intensity projection of a microglial cell. Red dots mark the ends of processes tracked with ImageJ. **b.** The velocities of the process ends from (**a**) shown over time. **c.** The distances the spots from (**a**) traveled from their starting points. **d.** The speed of 3 process ends tracked in 3D over time. **e**, **f** Graph showing the xyz positions of process ends from **d**. The heat legend shows passage of time, dark purple is frame 0, and light yellow is frame 12. The red dot represents the microglia soma.

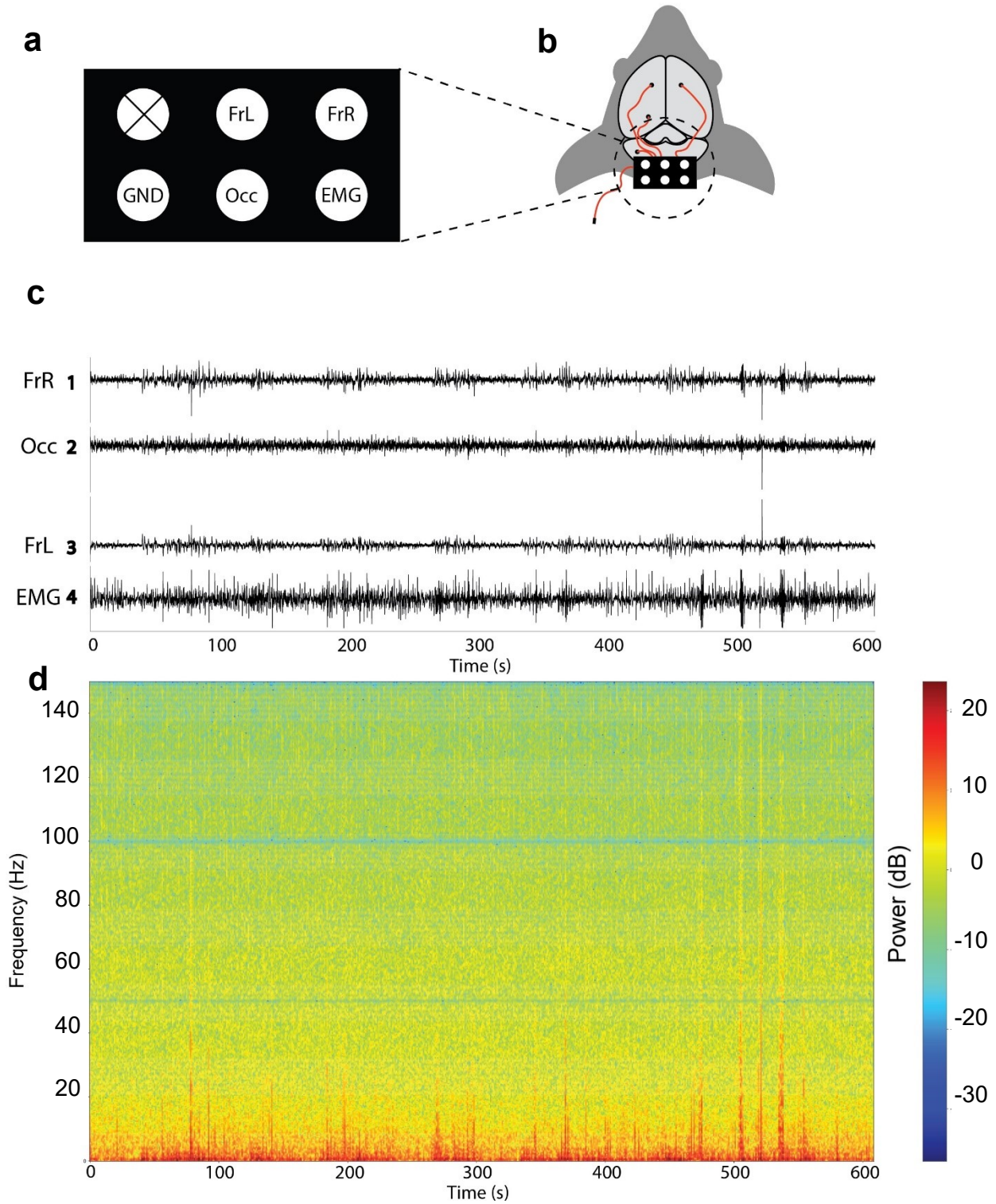

Figure 10: Electrode creation. a. Electrode pin map. Frontal Left = FrL; frontal right = FrR; ground, GND; Occipital = Occ; Electromyography = EMG; X = no pin. **b.** Illustration of electrode placement on mouse head. **c.** Example signals from the electrodes, no KA injection. **d.** Example stft plot of the same signals from **c**.

Part 3

3.4 Establishing EEG setup

The next part of this project was to establish electroencephalogram (EEG) recording, to compare the seizure activity to microglia dynamics. This was done by creating an electrode that would record from the frontal cortex, on the contralateral and ipsilateral side of where the imaging window would be, as well as a recording from the contralateral V1 (**Figure 10a**).

Figure 10c depicts EEG signals recorded from four different regions. These regions include: the frontal right (FrR) and frontal left (FrL) signals, which exhibit greater similarity to each other than to the occipital (Occ) signal, along with the electromyography (EMG) region. This suggests that the signal recorded from the Occ electrode will recapitulate the neuronal activity that occurs on the contralateral imaged side. The Short-time Fourier Transform (stft) plot in **Figure 10d** shows the power of the different frequencies of all the channels. There is low noise in this recording, which suggests that the electrode build successfully was able to record EEG signal from multiple brain regions, and that the signal to noise ratio is high enough to detect signal.

3.4.2 EEG noise reduction and filtering movement artifacts

Once the EEG setup was established, the next step was to assess the functionality of the recording setup at the (2-photon) 2P microscope. The microscope admits a lot of electrical noise, which could interfere with the EEG signal. Therefore, we tested for this by placing the electrode adapter itself under the 2P microscope. The EEG signal showed a rhythmic repetitive noise (**Figure 11a**) in all channels. The spectrogram and spectrum showed harmonics at 50 Hz intervals that reached a power of over 1000 $\mu V/\sqrt{Hz}$ (**Figure11b**, **c**). This kind of noise would overlay most of the EEG signal making it challenging to obtain the actual EEG signal. In order to reduce the noise, we built a Faraday cage, which is a grounding tool commonly used prevent electrostatic noise (Bielefeld et al., 2017) and obtain low-noise recordings. We designed a small one, which could fit around the mouse's body and under the microscope (**Figure 11g**). The Faraday cage resulted that no rhythmic noise in the EEG signal was recorded anymore (**Figure 11d-f**), which allowed us to record the neuronal signal and compare it to the microglial dynamics.

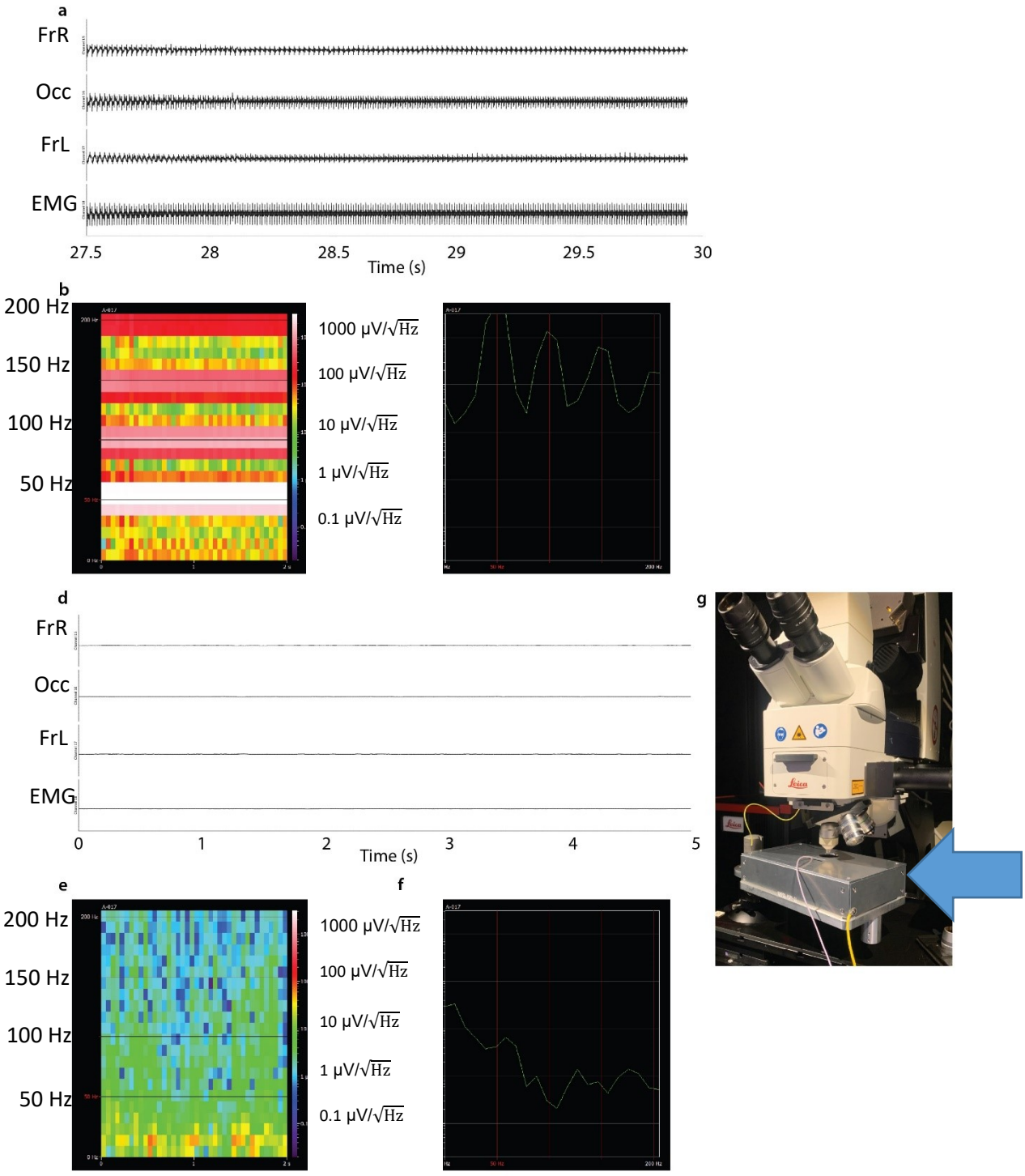

Figure 11: Faraday cage abolishes 50 Hz harmonic noise reduction of recordings. a. Recording from electrode placed under the 2-photon microscope without Faraday cage without mouse. **b.** Spectrogram showing 2 seconds from the EEG recording in (**a**). Harmonics shown at 50 Hz, 100 Hz, 150 Hz, and 200 Hz. **c.** Spectrum showing power of frequencies from one channel during recording in (a). **d.** Recording from electrode under the 2-photon microscope inside the Faraday cage, showing noise reduction. No mouse attached. **e.** Spectrogram showing 2 seconds from the EEG recording in (d). **f.** Spectrum showing power of frequencies from one channel during recording in (**d**) **g.** Image of Faraday cage under 2-photon microscope. Blue arrow indicates Faraday cage.

Part 4

3.5 Combining EEG with *in vivo* imaging

The length of imaging and EEG recording was set at about 2 hours to have sufficient time to develop seizures (**Figure 12a**). All of the mice reached stage 0 again within the last 20 minutes of observation (**Figure 4c**). This time window would allow for the comparison of microglia dynamics to multiple stages of seizure development.

The 2 hour imaging was split up into 4 windows, each about 30 minutes long. This allowed for manual drift correction between windows. The EEG recordings were also split into four time windows, to fit with the imaging windows (**Figure 12a**). After an initial 10 min baseline was recorded the mouse was briefly anesthetized with isoflurane, and then *i.p.* injected with KA. For the first two animals, a 20 mg/kg KA dose was injected based on the findings from **Figure 4c**. Both of these mice died within 30-60 minutes after injection, so we assumed that the added stress of head-fixing the mice was making them more susceptible to KA. Their EEG signal also showed powerful high frequency activity very soon after injection. Next we tested a lower dosage of 15 mg/kg, but this mouse died within the first hour as well.

Finally, we tried lower and sequential dosing. A previous study had shown that repeated administration of 5 mg/kg low doses of KA every 30 minutes allowed for a more controlled response to the KA, and a higher survival rate (Tse et al., 2014). Thus, we opted to administer the mouse with 10 mg/kg initially, followed by an additional 5 mg/kg dose, along with brief isoflurane anesthesia, after the first 30 minutes (**Figure 12a**). This approach resulted in a successful recording, which meant that the mouse survived, and progressed to having epileptic activity.

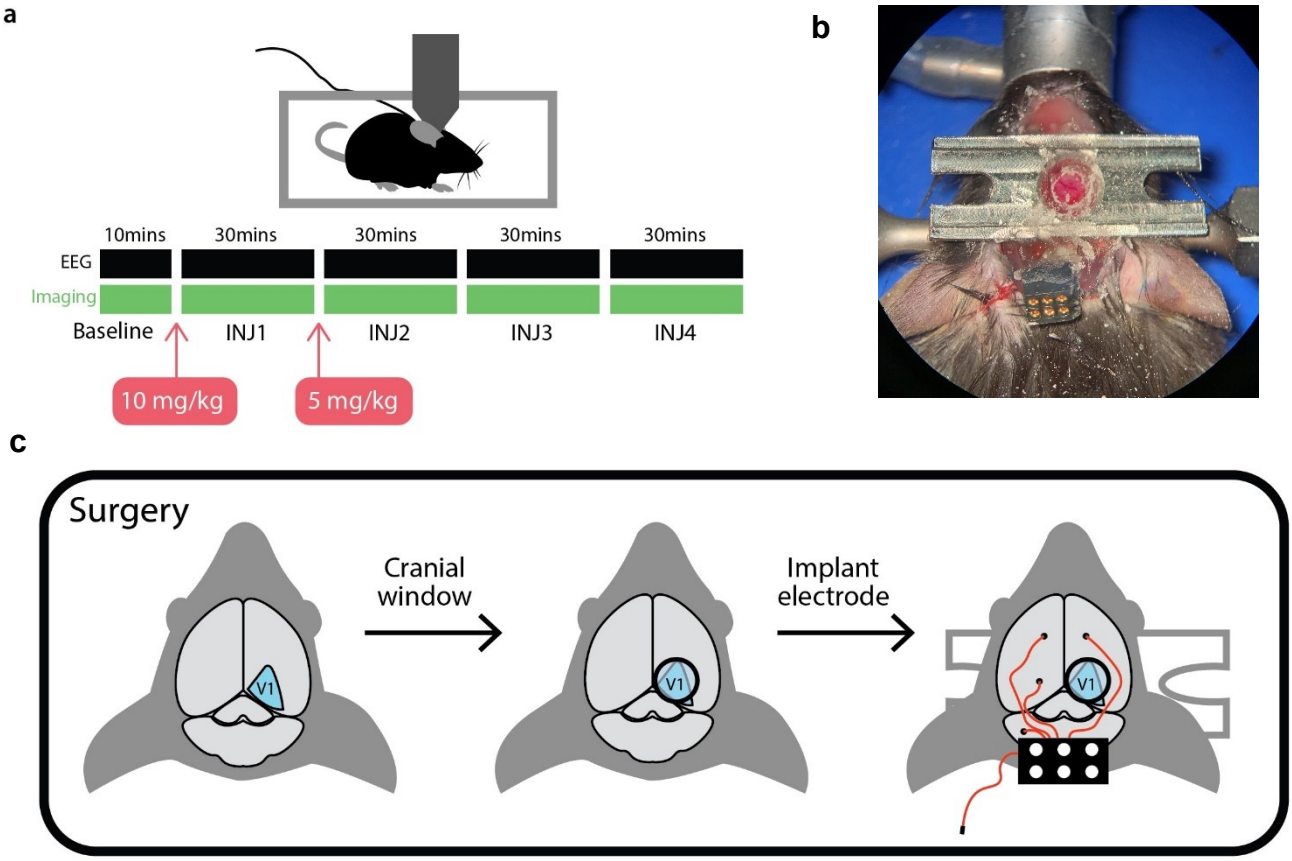

Figure 12: Surgery and imaging schematics. a. Timeline of imaging and EEG recordings. **b.** Image of mouse with both cranial window and electrode. **c.** Schematic showing surgery process. First the cranial window is attached and then the electrodes are implanted.

4.5.1 EEG signal after KA injection

When comparing seizure activity, we visually inspected the different features of the seizures. At baseline (**Figure 13c**) we observed low power oscillations in the EEG signal, with no bursts of high-power activity. After the initial KA injection there was a period of pre-ictal depression, with a lower signal power (**Figure 13b, 1**). This period of pre-ictal depression lasted about 22 minutes, followed by abnormal discharges of epileptiform activity (**Figure 13b, 2**). These abnormal discharges are followed directly by high-frequency bursts of pre-ictal activity to more frequent abnormal epileptic activity (**Figure 13b, 3**).

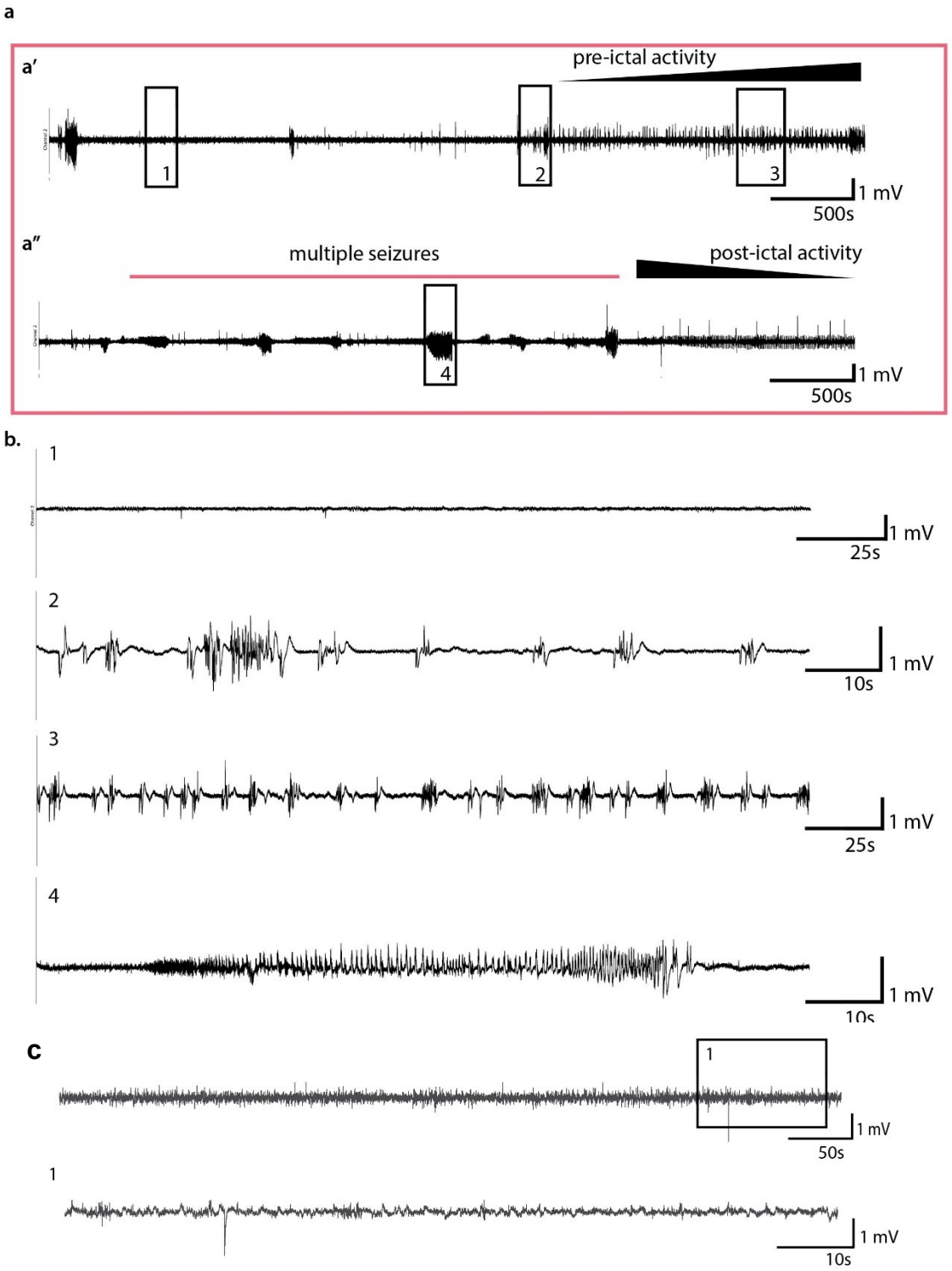

Figure 13: Epileptic activity progressed after KA injection. a. Example processed EEG signal after KA injection. **a'.** Shows first 30 minutes of recording after initial 10 mg KA injection. **a''** EEG signaling in second imaging window, right after second 5 mg/kg KA injection. **b.** Zoomed in portions of the signals shown in **(a). 1**. Pre-ictal depression after KA injection and before seizure activity. **2.** Abnormal discharges leading up to ictal activity. **3.** Pre-ictal activity. **4.** Epileptiform spikes. **c.** EEG signal of baseline. **1.** is zoomed in part of **c**.

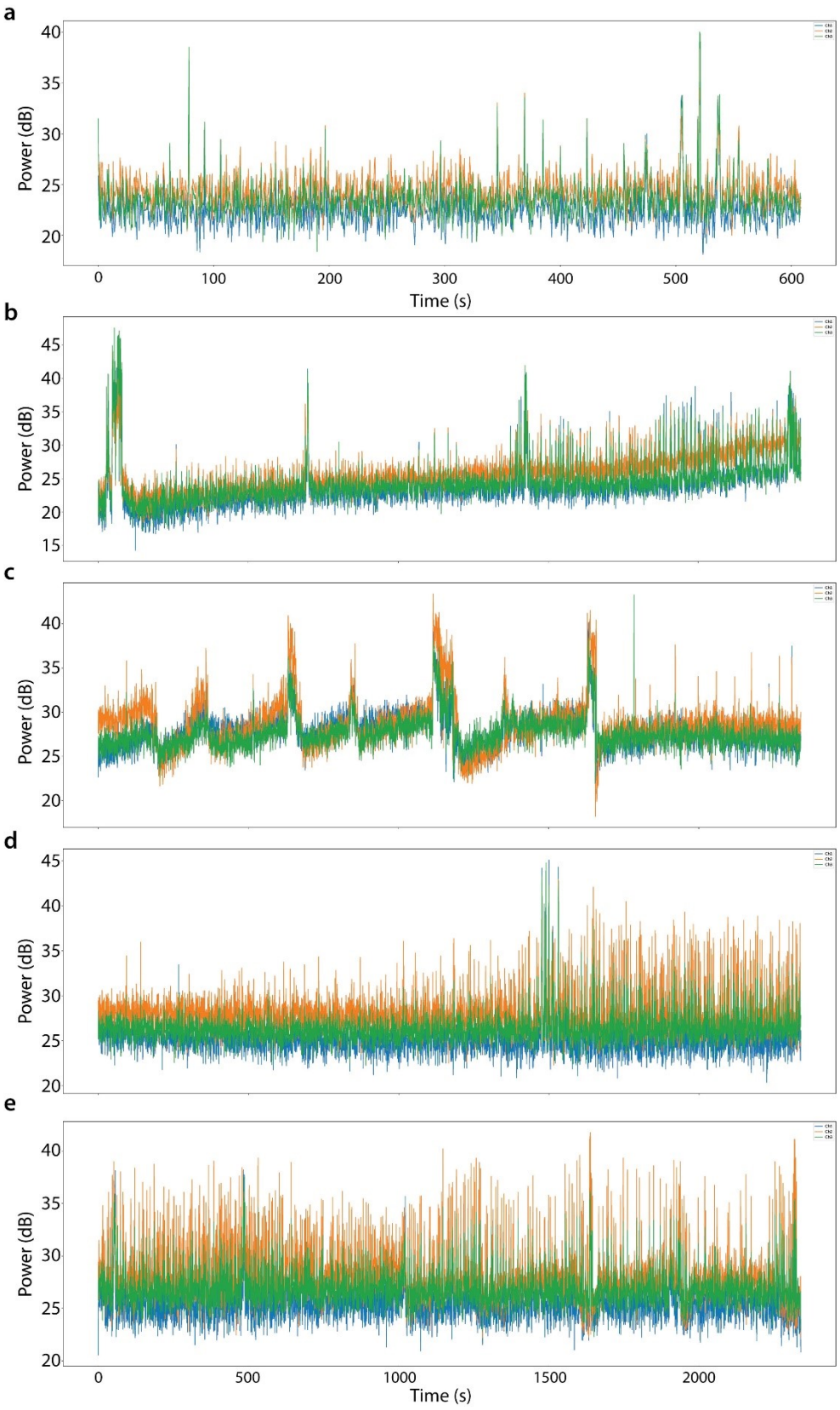

Figure 14: Gamma frequency spikes during seizures. a. Gamma frequency power at baseline. **b.** Gamma frequency after 10 mg/kg KA injection. **c.** Gamma frequency after 5 mg/kg KA injection **d.** Gamma frequency ~30 minutes after 5 mg/kg injection. **e.** Gamma frequency ~1 h after 5 mg/kg dose. Graphs show 3 channels, blue = frontal right lobe, orange = visual cortex, green = frontal left lobe.

After the subsequent injection of 5 mg/kg KA dose, multiple bursts of high-frequency epileptic activity lasting throughout the 30-minute imaging window occurred. To further delve into the intricacies of the EEG signal, we separated out different frequency ranges. We focused on the gamma frequency range (36-80 Hz). At baseline, the power of these frequencies stayed somewhat stable throughout the 10-minutes recording, with no clear rise or fall (**Figure 14a**). After the first 10 mg/kg dose of KA, the gamma frequencies increase steadily across the whole recording, and at about 22 minutes there are frequent power bursts of activity in this range (**Figure 14b**). This recapitulates the increase of abnormal epileptic activity seen in the overall EEG signal, and shows the change from pre-ictal depression into pre-ictal activity.

After the second dose of KA was applied, the gamma frequency signal exhibits seizure activity, with multiple pronounced increase in power from the beginning of the recording until 27 minutes into the recording (**Figure 14c**). After these sharp increases in gamma frequency power, the gamma frequencies stabilize and remain at a consistent level until the end of the recording. There are no additional significant rises in power observed in the gamma frequency for the remainder of the recording window.

In the third recording window, the gamma frequency power was stable until 25 minutes, where the gamma frequency high power bursts of activity until the end of the recording (**Figure 14d**).

In the last recording window, about 1.5 h after the first injection of KA, and about 2 h after the second injection, the gamma frequency still shows the high-power bursts of activity throughout the recording (**Figure 14e**).

3.5.1 Microglia volume changes with seizure activity

After the EEG and the 2P *in vivo* recording was successfully integrated, the next step was to directly compare the EEG signal with microglia dynamics. The first microglia parameter examined was the microglia volume change over time. This was done by comparing the total volume of microglia to the gamma power band (**Figure 15c-d**). At baseline, the gamma frequencies are stable, and no large increases are observed. There is a rise in volume at around the 6-minute mark (**Figure 15a**). This change in volume at baseline is much less strong than the change of volume in the subsequent imaging windows. In the initial imaging window, the volume decreases throughout the imaging. This change in volume has been normalized to the minimum and maximum values of the baseline, and ranges from the normalized value of 3.1 to -0.1. This is a three-fold increase in overall volume change (**Figure 15d**). This continues with the second imaging window, INJ2. The volume in this window fluctuates between the normalized values of -6.1 to -2.3. This represents an almost 4 -fold increase in the range of volume change compared to baseline (**Figure 15d**). This pattern changes in INJ3, where the overall volume range is nearly equal to one, similar to the overall volume change at

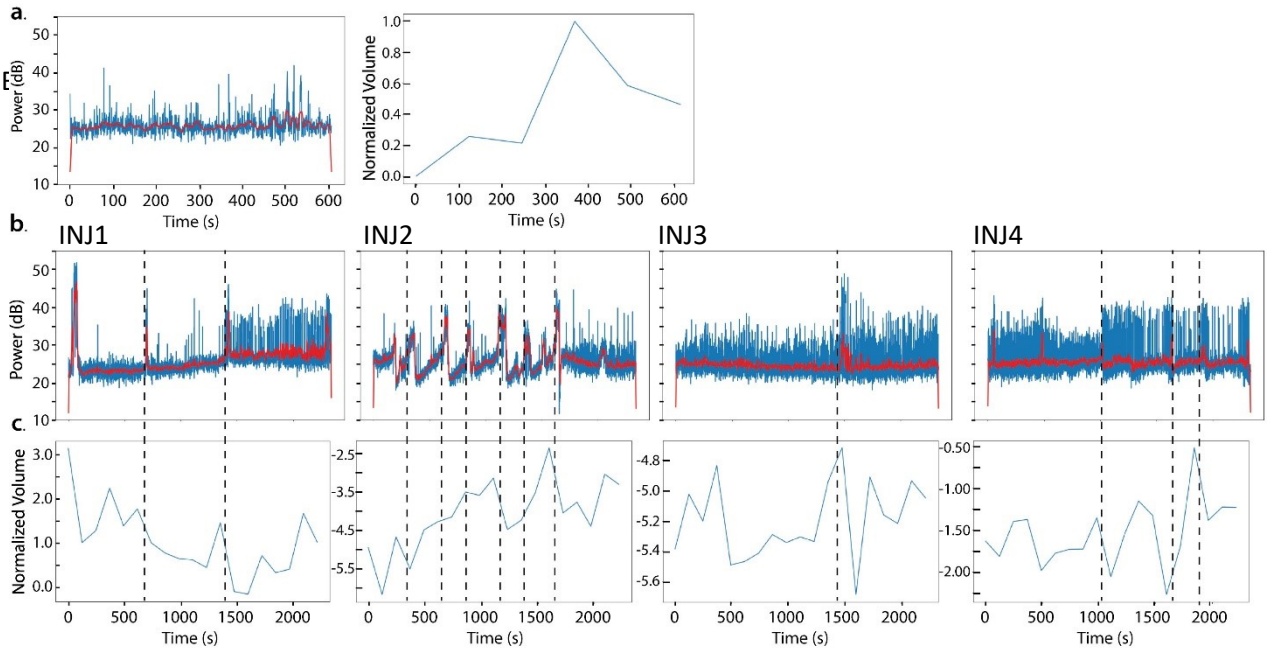

Figure 15: Microglia volume of change visually changes with increased gamma frequency power. a. Baseline gamma frequency plot, and microglia volume change. **b.** Gamma frequency plots of EEG activity from one mouse during four recording windows (INJ1, INJ2, INJ3, INJ4). **c.** Microglia total volume across the same recording windows. Microglia volume is normalized to the maximum and minimum volumes at baseline.

baseline. At INJ4 the range increases again, growing to 1.75 times larger than the range observed at baseline (**Figure 15d**). When directly comparing the gamma band power to the changes in volume of microglia, there were 12 main events marked that show strong changes in the power of the gamma band. When visually inspected, 9 out of the 12 events coincide with drops in microglia volume (**Figure 15c-d**), although no strong associations can be made. The overall volume is not compared between imaging windows, as there were slight variations with the acquisition windows that could cause volume to be lost or added between each recording.

The next step was to attempt to correlate the microglia volume change with changes in the EEG power. The overall EEG signal was binned into windows that coincided with the acquired 2P microscope images. At baseline, the volume increases before the EEG power increases, and decreases slightly once the EEG signal has increased (**Figure 16a**). There is no obvious visual correlation. The Pearson's correlation value between these two values was found to be 0.034, showing no correlation. At INJ1 the microglia volume decreases across the recording, while the mean EEG power increases, starting at around 25 minutes (**Figure 16b**). The Pearson's correlation value was 0.178, a very low correlation. The next recording window shows a high correlation with a Pearson's coefficient of 0.682. Here, there are two large spikes in EEG amplitude that are captured by the binning, and these increases in power are clearly

followed by increases in microglia volume. During the 16 minutes preceding the first large spike in EEG power, the microglia volume steadily increases. This upward trend stops during the spike in EEG mean power and drops back down after the EEG power decreases again. Subsequently, the volume rapidly rises again following the second large spike in EEG power (**Figure 16c**). In INJ3 there is one large spike in EEG power, that is also followed by a peak in microglia volume. This correlation was found to be low, with a Pearson's value of 0.350 (**Figure 16d**). Finally, the last recording window showed fluctuations in EEG power. There are three increases in signal power, while the microglia volume fluctuates many times. No correlation was found, with a Pearson's correlation value of 0.054 (**Figure 16e**).

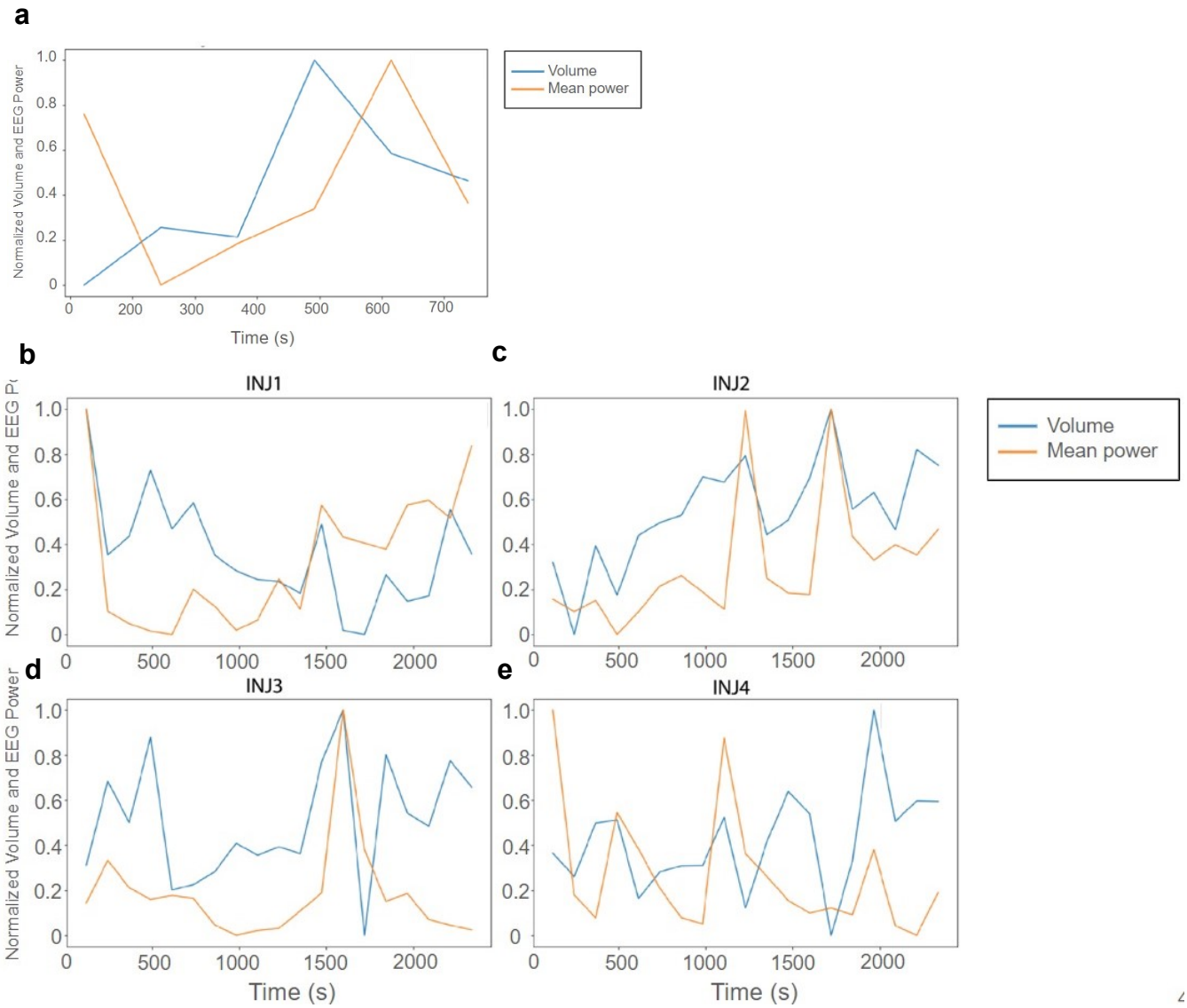

Figure 16: Microglia volume of change visually shows relationship with EEG signal power. a. Microglia volume and EEG signal at baseline. **b.** Microglia volume and EEG signal in time window 1 (INJ1) after 10 mg/kg injection. **c.** Microglia volume and EEG in time window 2 (INJ2) after 5 mg/kg injection. **d.** Microglia volume and EEG signal in time window 3 (INJ3). **e.** Microglia volume and EEG signal at baseline in time window 4 (INJ4). Yellow = mean power, blue = microglia volume.

4. Discussion

Epilepsy is a neurological disorder that is characterized by hyper-synchrony of neuronal activity, as well as hyper-excitability of neurons that leads to recurrent seizures (Fisher et al., 2005). Despite multiple antiepileptic drugs available, the success of those drugs to manage the disease symptoms have been unsatisfying (Eyo et al., 2017; Engel et al., 2012). This highlights gaps in our understanding of the underlying mechanisms that controls epilepsy, as these treatments focus mainly on the neuronal aspect of epilepsy. Although the regulation of neuronal activity in the brain has long been viewed as a disease exclusively involving neurons, recent studies have suggested a substantial contribution of microglia to this process (Li et al., 2012; Eyo et al., 2014; Akiyoshi et al., 2018; Wake et al., 2009; Feng et al., 2019; Cserép et al., 2020; Badimon et al., 2020). Microglia response to acute seizures can help our understanding of how microglia contribute to or mitigate the development of epilepsy. Two-photon (2P) *in vivo* imaging enables detailed analysis of microglial morphology and dynamics during acute seizures, and electroencephalogram (EEG) analysis helps define seizure characteristics and neuronal activity patterns. 2P *in vivo* imaging enables detailed analysis of microglial morphology and dynamics during acute seizures, providing insights into microglia-neuron interactions and their functional consequences. Understanding microglia dynamics during seizures holds promise for elucidating epilepsy mechanisms.

In this study, we aimed to integrate 2P and EEG recording to be able to eventually compare specific microglia dynamic and morphological changes with seizure occurrence, as well as seizure severity, using the kainic acid (KA) model of temporal lobe epilepsy (TLE).

4.1 Microglia activation after KA injection

As a first step, we wanted to determine the optimal dosage of KA for *in vivo* imaging. Our results suggested that the 20 mg/kg dosage would be the ideal dosage within the range of not being too severe and not at all effective. From this experiment we determined a dosage curve for KA. We observed that an increase in KA dosage corresponds to an increase in seizure severity, although with considerable variability across mice. This fits aligns with previous findings indicating that C57BL/6 mice are resistant to KA administration, as well as experience high variability in response to KA injection (McKhann et al., 2003).

The next step was to check if the microglia become activated at certain doses of KA. To do this, we stained for CD68 and calculated the percent volume of CD68 within the microglia (**Figure 6**). The resulting data showed no significant differences in percent volume of CD68 within microglia between KA doses and the control. Although, there was an increase in the varying doses, but with a large variability at the 10 mg/kg dosage.

This could be due to the fact that more mice would need to be used to get a more accurate look at CD68 expression. There does seem to be an increase in CD68 expression in the visual cortex (V1) 2 h after KA injection, but it does not seem to increase with increasing dosage.

Previous studies showed that the CD68 expression was increased after *status epilepticus* (SE) (Abiega et al., 2016). Abiega found that it increased until it reached its peak expression 7 days after KA injection, but not at 4 hours after injection. Our results suggest that there is a slight increase in CD68 expression 2 hours after KA injection, but as it does not correlate with increasing KA dose, other factors could be in play. In one recent study, using the unilateral intracoritcal KA model, they showed that in the CA1 brain area, CD68 is significantly upregulated 5 days after KA injection but not upregulated 4 h after injection (Henning et al., 2022). They concluded that microglia acquire a reactive phenotype after KA-induced SE, and that the microglia do in fact become rapidly reactive before the onset of neurodegeneration. This project focuses on the direct effects of SE on microglial dynamics before neurodegeneration. Our CD68 data fits into these two studies. Although we did not see a significant increase in CD68 expression in the V1. We did observe an increase in ramification in the V1 at the 30 mg/kg dose (**Figure 5c**), and a more activated phenotype in the DG and CA3 regions at the 20 and 30 mg/kg dose (**Figure 5a,b**). The hyper-ramification observed in microglia is in agreement with previous studies (Rappold et al., 2006; Eyo et al., 2014). This state had been previously found to occur as early as 40 minutes after KA treatment by both intraperitoneal and intracerebroventricular routes (Eyo et al., 2014). The same study recapitulated these results by bath application of glutamate/NMDA to acute brain slices. Another study independently reported similar results, and found that microglia respond within 5-10 minutes to neuronal hyperactivity triggered by activation of NMDA glutamate receptors with bath application of glutamate to acute brain slices (Dissing-Olsen et al., 2014).

In summary, we were able to show microglia morphological changes in the V1, DG, and CA3 within 2 hours of KA injection at 20 mg/kg and 30 mg/kg dose. And although, we were not able to see obvious changes in microglia morphology at the 20 mg/kg dose in the V1, the goal was to observe dynamic changes in microglia in response to seizure activity *in vivo*, and thus the 20 mg/kg dose was determined to be the best suited for this.

4.2 Integration of 2-photon imaging and EEG recording

We integrated EEG recording with *in vivo* 2P imaging to examine the relationship between acute seizure activity and microglial dynamics. Initially, our experiments with the 20 mg/kg KA dose resulted in mouse mortality within 30-60 minutes post-injection, likely exacerbated by the stress of head-fixing, as well as the implanted electrodes. A previous study showed that mice with electrodes implanted need about 40% less KA to induce convulsive SE than mice without (Sharma et al., 2018). Subsequent exploration of lower KA dosages led to the successful implementation of repeated dosing strategy, with an initial 10 mg/kg injection followed by an additional 5 mg/kg dose after the initial imaging window of about 30 minutes. This resulted in sustained epileptic activity. In the future, the dosage response curve would need to be more carefully tested, taking into account factors such surgical manipulations and stress and not just age, sex, and circadian rhythms.

The EEG signal following KA injection revealed distinct patterns of pre-ictal depression, which preceded abnormal epileptiform spike activity, followed by bursts of high-frequency epileptic activity. Notably, the power of the gamma frequency band exhibited fluctuations corresponding to the onset and progression of seizure activity. This steep rise in gamma is in line with previous findings, where signal in the gamma frequency increased during stage 3 seizures (Sharma et al., 2018).

When correlating the increase in microglial volume with the power of the EEG signal, we observed no strong correlation between the binned EEG signal and overall microglia volume. The Pearson's correlation values for all injection windows were higher than those at baseline. However, further in-depth analysis is required to draw definitive conclusions from this data. The mean EEG power was binned into intervals equivalent to the duration of imaging one frame, simplifying the analysis of the EEG signal complexity while facilitating a comparison between the two datasets. The next step would be to compare the gamma frequency power to the microglia volume. Future steps involve correlating the speed and extension retraction of microglia processes, though this may require additional time or the development of new tracking methods to alleviate the time-intensive manual tracking process.

4.3 Technical challenges

After the EEG recording set up was successfully implemented, there was still some filtering needed to reduce the noise even after the Faraday cage was built. One reason for this was because the electrode connector was attached to the back of the mouse's head, and allowed the back of the mouse to sometimes come into contact with the connector. This led to some

movement artifacts, that were difficult to filter out. In the future the connector could be attached to the side of the mouse's head, so that the back of the mouse had less of a chance to touch it.

Movement artifacts were also an issue with the 2P imaging. It took about two minutes to acquire a z-stack, which meant that if there were slight movements during the imaging of one z-stack it would shift the images in the z-axis. Further methods would need to be developed to be able to fix this issue in post processing. This issue contributed to delays in the analysis, and could affect the volume data fluctuations. Smaller faster z-stacks could help mitigate this problem. Another method that could ease the process of tracking individual microglia would be having a GFP label that is less highly expressed. This way microglia would be more distributed, and their individual processes and volumes could be more easily separated.

When comparing microglial volume changes to seizure activity, we observed dynamic alterations in volume following KA injection (**Figure 16**). Drops in microglial volume rougly coincided with increases in gamma power, suggesting a potential relationship between microglial volume and seizure activity. However, the movement of the mouse during the imaging shifted the cells, and could contribute to the slight correlation we observed.

In conclusion, our study successfully implemented 2P imaging and EEG recording to investigate microglial dynamics during epileptic activity. While preliminary correlations between microglial volume increase and EEG power were observed, further in-depth analysis and correlation of microglial process dynamics with EEG signals are warranted. Future research endeavors will benefit from refining experimental methodologies and delving deeper into the intricate interplay between microglia and neuronal activity in epilepsy pathophysiology.

4.4 Future outlook

Recent advancements in epilepsy research have led to a notable shift towards a vascular-centered concept of epileptogenesis. One critical aspect of this shift involves investigating the role of increased blood-brain barrier (BBB) permeability in the pathophysiology of epilepsy, as highlighted in studies such as Prager et al. (2019). This emerging perspective prompts exploration into how microglia, interact with the vasculature and respond to changes in BBB permeability.

Additionally, the use of transgenic mice expressing both Thy1 labels and CX3CR1-GFP provides a valuable model for studying microglia-neuron interactions. Specifically, researchers can examine microglial phagocytosis of neurons and the intricate contacts formed between microglia and neurons to elucidate their dynamic relationship.

Despite the insights gained from analyzing microglia morphology, it is essential to recognize the limitations of relying solely on this approach to understand real-time changes. While physical contacts between microglia and neurons (Davalos et al., 2005; Nimmerjahn et al., 2005) offers valuable information, it is crucial to supplement morphology analysis with functional modalities, to help understand what the changes in morphology are doing. This integration allows for a more comprehensive understanding of microglial responses in various pathological contexts. Calcium signaling of microglia is elevated under conditions of pathology and altered neuronal activity (Eichhoff, Brawek, & Garaschuk, 2011; Pozner et al., 2015; Umpierre et al., 2020) and has been linked to phagocytic function *in situ* and *in vivo* (Koizumi et al., 2007; Neher et al., 2014). Examining changes in calcium activity in microglia during morphological alterations could assist us in understanding the inter- and intra-cellular communication that occurs between microglia processes and neurons (Umpierre et al., 2021).

In conclusion, integrating methods that tell us structure of microglia and the function of the structure can help in advancing our understanding of the intricate interactions between microglia and neurons, particularly in the context of epilepsy pathophysiology.

5. References

Abiega, O., Beccari, S., Diaz-Aparicio, I., Nadjar, A., Layé, S., Leyrolle, Q., Gómez-Nicola, D., Domercq, M., Pérez-Samartín, A., Sánchez-Zafra, V., Paris, I., Valero, J., Savage, J. C., Hui, C.-W., Tremblay, M.-È., Deudero, J. J. P., Brewster, A. L., Anderson, A. E., Zaldumbide, L., … Sierra, A. (2016). Neuronal Hyperactivity Disturbs ATP Microgradients, Impairs Microglial Motility, and Reduces Phagocytic Receptor Expression Triggering Apoptosis/Microglial Phagocytosis Uncoupling. *PLoS Biology*, *14*(5), e1002466. https://doi.org/10.1371/journal.pbio.1002466

Ahlers, K. E., Karacay, B., Fuller, L., Bonthius, D. J., & Dailey, M. E. (2015). Transient activation of microglia following acute alcohol exposure in developing mouse neocortex is primarily driven by BAX-dependent neurodegeneration. *Glia*. doi: 10.1002/glia.22835

Akiyoshi, R., Wake, H., Kato, D., Horiuchi, H., Ono, R., Ikegami, A., Haruwaka, K., Omori, T., Tachibana, Y., Moorhouse, A. J., & Nabekura, J. (2018). Microglia Enhance Synapse Activity to Promote Local Network Synchronization. *eNeuro*, *5*(5), ENEURO.0088-18.2018. https://doi.org/10.1523/ENEURO.0088-18.2018

Augusto-Oliveira, M., Arrifano, G. P., Delage, C. I., Tremblay, M.-È., Crespo-Lopez, M. E., & Verkhratsky, A. (2022). Plasticity of microglia. *Biological Reviews*, *97*(1), 217–250. https://doi.org/10.1111/brv.12797

Avignone, E., Lepleux, M., Angibaud, J., & Nägerl, U. V. (2015). Altered morphological dynamics of activated microglia after induction of status epilepticus. Journal of Neuroinflammation, 12(1), 202. https://doi.org/10.1186/s12974-015-0421-6

Avignone, E., Ulmann, L., Levavasseur, F., Rassendren, F., & Audinat, E. (2008). Status Epilepticus Induces a Particular Microglial Activation State Characterized by Enhanced Purinergic Signaling. *The Journal of Neuroscience*, *28*(37), 9133–9144. https://doi.org/10.1523/JNEUROSCI.1820-08.2008

Badimon, A., Strasburger, H. J., Ayata, P., Chen, X., Nair, A., Ikegami, A., Hwang, P., Chan, A. T., Graves, S. M., Uweru, J. O., Ledderose, C., Kutlu, M. G., Wheeler, M. A., Kahan, A., Ishikawa, M., Wang, Y.-C., Loh, Y.-H. E., Jiang, J. X., Surmeier, D. J., … Schaefer, A. (2020). Negative feedback control of neuronal activity by microglia. *Nature*, *586*(7829), Article 7829. https://doi.org/10.1038/s41586-020-2777-8

Beach, T. G., Woodhurst, W. B., MacDonald, D. B., & Jones, M. W. (1995). Reactive microglia in hippocampal sclerosis associated with human temporal lobe epilepsy. *Neuroscience Letters*, *191*(1–2), 27–30. https://doi.org/10.1016/0304-3940(94)11548-1

Ben-Ari, Y., & Cossart, R. (2000). Kainate, a double agent that generates seizures: Two decades of progress. *Trends in Neurosciences, 23*(11), 580–587. https://doi.org/10.1016/S0166-2236(00)01659-3

Bielefeld, P., Sierra, A., Encinas, J. M., Maletic-Savatic, M., Anderson, A., & Fitzsimons, C. P. (2017). A Standardized Protocol for Stereotaxic Intrahippocampal Administration of Kainic Acid Combined with Electroencephalographic Seizure Monitoring in Mice. *Frontiers in Neuroscience*, *11*, 160. https://doi.org/10.3389/fnins.2017.00160

Boer, K., Spliet, W. G. M., van Rijen, P. C., Redeker, S., Troost, D., & Aronica, E. (2006). Evidence of activated microglia in focal cortical dysplasia. *Journal of Neuroimmunology*, *173*(1–2), 188–195. https://doi.org/10.1016/j.jneuroim.2006.01.002

Broekaart, D. W. M., Anink, J. J., Baayen, J. C., Idema, S., de Vries, H. E., Aronica, E., Gorter, J. A., & van Vliet, E. A. (2018). Activation of the innate immune system is evident throughout epileptogenesis and is associated with blood-brain barrier dysfunction and seizure progression. *Epilepsia*, *59*(10), 1931–1944. https://doi.org/10.1111/epi.14550

Cardona AE, Pioro EP, Sasse ME, Kostenko V, Cardona SM, Dijkstra IM, Huang D, Kidd G, Dombrowski S, Dutta R, Lee JC, Cook DN, Jung S, Lira SA, Littman DR, Ransohoff RM (2006) Control of microglial neurotoxicity by the fractalkine receptor. Nat Neurosci 9:917–924.

Choi, J., & Koh, S. (2008). Role of Brain Inflammation in Epileptogenesis. *Yonsei Medical Journal*, *49*(1), 1–18. https://doi.org/10.3349/ymj.2008.49.1.1

Colombo, G., Cubero, R. J. A., Kanari, L., Venturino, A., Schulz, R., Scolamiero, M., Agerberg, J., Mathys, H., Tsai, L.-H., Chachólski, W., Hess, K., & Siegert, S. (2022). A tool for mapping microglial morphology, morphOMICs, reveals brain-region and sex-dependent phenotypes. *Nature Neuroscience*, *25*(10), 1379–1393. https://doi.org/10.1038/s41593-022-01167-6

Cserép, C., Pósfai, B., Lénárt, N., Fekete, R., László, Z. I., Lele, Z., Orsolits, B., Molnár, G., Heindl, S., Schwarcz, A. D., Ujvári, K., Környei, Z., Tóth, K., Szabadits, E., Sperlágh, B., Baranyi, M., Csiba, L., Hortobágyi, T., Maglóczky, Z., … Dénes, Á. (2020). Microglia monitor and protect neuronal function through specialized somatic purinergic junctions. Science (New York, N.Y.), 367(6477), 528–537. https://doi.org/10.1126/science.aax6752

Cunningham, C. (2013). Microglia and neurodegeneration: The role of systemic inflammation. *Glia*, *61*(1), 71–90. https://doi.org/10.1002/glia.22350

Davalos, D., Grutzendler, J., Yang, G., Kim, J. V., Zuo, Y., Jung, S., Littman, D. R., Dustin, M. L., & Gan, W.-B. (2005). ATP mediates rapid microglial response to local brain injury *in vivo*. *Nature Neuroscience*, *8*(6), Article 6. https://doi.org/10.1038/nn1472

Dissing-Olesen, L., LeDue, J. M., Rungta, R. L., Hefendehl, J. K., Choi, H. B., & MacVicar, B. A. (2014). Activation of Neuronal NMDA Receptors Triggers Transient ATP-Mediated Microglial Process Outgrowth. *The Journal of Neuroscience*, *34*(32), 10511–10527. https://doi.org/10.1523/JNEUROSCI.0405-14.2014

Douma, K., Megens, R. T. A., Reitsma, S., Prinzen, L., Slaaf, D. W., & Van Zandvoort, M. A. M. J. (2007). Two-photon lifetime imaging of fluorescent probes in intact blood vessels: A window to sub-cellular structural information and binding status. *Microscopy Research and Technique*, *70*(5), 467–475. https://doi.org/10.1002/jemt.20424

Eichhoff, G., Brawek, B., & Garaschuk, O. (2011). Microglial calcium signal acts as a rapid sensor of single neuron damage *in vivo*. *Biochimica et Biophysica Acta*, 1813(5), 1014–1024. doi:10.1016/j.bbamcr.2010.10.018

Ekdahl, C. T. (2012). Microglial Activation – Tuning and Pruning Adult Neurogenesis. *Frontiers in Pharmacology*, *3*. https://doi.org/10.3389/fphar.2012.00041

- User License: Attribution- 4.0 International (CC BY-NC-ND 4.0), Non Commercial, No Derivatives, Publisher: Frontiers

Engel, J. (2001). Mesial Temporal Lobe Epilepsy: What Have We Learned? *The Neuroscientist*, *7*(4), 340–352. https://doi.org/10.1177/107385840100700410

Engel, T., Gomez-Villafuertes, R., Tanaka, K., Mesuret, G., Sanz-Rodriguez, A., Garcia-Huerta, P., Miras-Portugal, M. T., Henshall, D. C., & Diaz-Hernandez, M. (2012). Seizure suppression and neuroprotection by targeting the purinergic P2X7 receptor during status epilepticus in mice. *The FASEB Journal*, *26*(4), 1616–1628. https://doi.org/10.1096/fj.11-196089

Eyo, U. B., Miner, S. A., Weiner, J. A., & Dailey, M. E. (2016). Developmental changes in microglial mobilization are independent of apoptosis in the neonatal mouse hippocampus. *Brain, Behavior, and Immunity*, *55*, 49–59. https://doi.org/10.1016/j.bbi.2015.11.009

Eyo, U. B., Murugan, M., & Wu, L.-J. (2017). Microglia–Neuron Communication in Epilepsy. *Glia*, *65*(1), 5–18. https://doi.org/10.1002/glia.23006

Eyo, U. B., Peng, J., Swiatkowski, P., Mukherjee, A., Bispo, A., & Wu, L.-J. (2014). Neuronal Hyperactivity Recruits Microglial Processes via Neuronal NMDA Receptors and Microglial P2Y12 Receptors after Status Epilepticus. *Journal of Neuroscience*, *34*(32), 10528–10540. https://doi.org/10.1523/JNEUROSCI.0416-14.2014

Feng, L., Murugan, M., Bosco, D. B., Liu, Y., Peng, J., Worrell, G. A., Wang, H.-L., Ta, L. E., Richardson, J. R., Shen, Y., & Wu, L.-J. (2019). Microglial Proliferation and Monocyte Infiltration Contribute to Microgliosis following Status Epilepticus. *Glia*, *67*(8), 1434–1448. https://doi.org/10.1002/glia.23616

Fisher, R. S., Boas, W. van E., Blume, W., Elger, C., Genton, P., Lee, P., & Engel Jr., J. (2005). Epileptic Seizures and Epilepsy: Definitions Proposed by the International League Against Epilepsy (ILAE) and the International Bureau for Epilepsy (IBE). *Epilepsia*, *46*(4), 470–472. https://doi.org/10.1111/j.0013-9580.2005.66104.x

Gaitatzis, A., Johnson, A. L., Chadwick, D. W., Shorvon, S. D., & Sander, J. W. (2004). Life expectancy in people with newly diagnosed epilepsy. *Brain: A Journal of Neurology*, *127*(Pt 11), 2427–2432. https://doi.org/10.1093/brain/awh267

Hanisch, UK., Kettenmann, H. Microglia: active sensor and versatile effector cells in the normal and pathologic brain. *Nat Neurosci* **10**, 1387–1394 (2007). https://doi.org/10.1038/nn1997

Haynes, S. E., Hollopeter, G., Yang, G., Kurpius, D., Dailey, M. E., Gan, W.-B., & Julius, D. (2006). The P2Y12 receptor regulates microglial activation by extracellular nucleotides. *Nature Neuroscience*, *9*(12), 1512–1519. https://doi.org/10.1038/nn1805

Helmchen, F., & Denk, W. (2005). Deep tissue two-photon microscopy. *Nature Methods*, *2*(12), 932–940. https://doi.org/10.1038/nmeth818

Henning, L., Antony, H., Breuer, A., Müller, J., Seifert, G., Audinat, E., Singh, P., Brosseron, F., Heneka, M. T., Steinhäuser, C., & Bedner, P. (2022). Reactive microglia are the major source of tumor necrosis factor alpha and contribute to astrocyte dysfunction and acute seizures in experimental temporal lobe epilepsy. Glia). https://doi.org/10.1002/glia.24265

Huguenard, J., & MacCormick, D. A. (1994). Electrophysiology of the neuron: An interactive tutorial; [Macintosh version]. Oxford Univ. Press.

Ji, K., Akgul, G., Wollmuth, L. P., & Tsirka, S. E. (2013). Microglia actively regulate the number of functional synapses. *PloS One*, *8*(2), e56293. https://doi.org/10.1371/journal.pone.0056293

Jung, S., Aliberti, J., Graemmel, P., Sunshine, M. J., Kreutzberg, G. W., Sher, A., & Littman, D. R. (2000). Analysis of Fractalkine Receptor CX3CR1 Function by Targeted Deletion and Green

Fluorescent Protein Reporter Gene Insertion. *Molecular and Cellular Biology*, *20*(11), 4106–4114.

Jurga, A. M., Paleczna, M., & Kuter, K. Z. (2020). Overview of General and Discriminating Markers of Differential Microglia Phenotypes. *Frontiers in Cellular Neuroscience*, *14*, 198. https://doi.org/10.3389/fncel.2020.00198

Kandratavicius, L., Balista, P. A., Lopes-Aguiar, C., Ruggiero, R. N., Umeoka, E. H., Garcia-Cairasco, N., Bueno-Junior, L. S., & Leite, J. P. (2014). Animal models of epilepsy: Use and limitations. *Neuropsychiatric Disease and Treatment*, *10*, 1693–1705. https://doi.org/10.2147/NDT.S50371

Kettenmann, H., Kirchhoff, F., & Verkhratsky, A. (2013). Microglia: New roles for the synaptic stripper. *Neuron*, *77*(1), 10–18. https://doi.org/10.1016/j.neuron.2012.12.023

Khan, L., van Lanen, R., Hoogland, G., Schijns, O., Rijkers, K., Kapsokalyvas, D., van Zandvoort, M., & Haeren, R. (2021). Two-Photon Imaging to Unravel the Pathomechanisms Associated with Epileptic Seizures: A Review. *Applied Sciences*, *11*(5), Article 5. https://doi.org/10.3390/app11052404

Kim, B., Ding, W., Yang, L., Chen, Q., Mao, J., Feng, G., Choi, J. H., & Shen, S. (2024). Simultaneous two-photon imaging and wireless EEG recording in mice. *Heliyon*, *10*(5), e25910. https://doi.org/10.1016/j.heliyon.2024.e25910

Koizumi, S., Shigemoto-Mogami, Y., Nasu-Tada, K., Shinozaki, Y., Ohsawa, K., Tsuda, M., Joshi, B. V., Jacobson, K. A., Kohsaka, S., & Inoue, K. (2007). UDP acting at P2Y6 receptors is a mediator of microglial phagocytosis. *Nature*, *446*(7139), 1091–1095. https://doi.org/10.1038/nature05704

Kyle, J. J., Sharma, S., Tiarks, G., Rodriguez, S., & Bassuk, A. G. (2023). Fast Detection and Quantification of Interictal Spikes and Seizures in a Rodent Model of Epilepsy Using an Automated Algorithm. *Bio-Protocol*, *13*(6), e4632. https://doi.org/10.21769/BioProtoc.4632

Kyrargyri, V., Attwell, D., Jolivet, R. B., & Madry, C. (2019). Analysis of Signaling Mechanisms Regulating Microglial Process Movement. In O. Garaschuk & A. Verkhratsky (Eds.), *Microglia: Methods and Protocols* (pp. 191–205). Springer. https://doi.org/10.1007/978-1-4939-9658-2_14

Leite, J. P., Garcia-Cairasco, N., & Cavalheiro, E. A. (2002). New insights from the use of pilocarpine and kainate models. *Epilepsy Research*, *50*(1–2), 93–103. https://doi.org/10.1016/s0920-1211(02)00072-4

Lévesque, M., & Avoli, M. (2013). The kainic acid model of temporal lobe epilepsy. *Neuroscience & Biobehavioral Reviews*, *37*(10, Part 2), 2887–2899. https://doi.org/10.1016/j.neubiorev.2013.10.011

Li, Y., Du, X., Liu, C., Wen, Z., & Du, J. (2012). Reciprocal Regulation between Resting Microglial Dynamics and Neuronal Activity In Vivo. *Developmental Cell*, *23*(6), 1189–1202. https://doi.org/10.1016/j.devcel.2012.10.027

Lisgaras, C. P., & Scharfman, H. E. (2022). Robust chronic convulsive seizures, high frequency oscillations, and human seizure onset patterns in an intrahippocampal kainic acid model in mice. *Neurobiology of Disease*, *166*, 105637. https://doi.org/10.1016/j.nbd.2022.105637

Meisler, M. H., Kearney, J., Ottman, R., & Escayg, A. (2001). IDENTIFICATION OF EPILEPSY GENES IN HUMAN AND MOUSE. Annual Review of Genetics, 35, 567–588. https://doi.org/10.1146/annurev.genet.35.102401.091142

McKhann, G. M., Wenzel, H. J., Robbins, C. A., Sosunov, A. A., & Schwartzkroin, P. A. (2003). Mouse strain differences in kainic acid sensitivity, seizure behavior, mortality, and hippocampal pathology. Neuroscience, 122(2), 551–561. https://doi.org/10.1016/s0306-4522(03)00562-1

Merlini, M., Rafalski, V. A., Ma, K., Kim, K.-Y., Bushong, E. A., Rios Coronado, P. E., Yan, Z., Mendiola, A. S., Sozmen, E. G., Ryu, J. K., Haberl, M. G., Madany, M., Sampson, D. N., Petersen, M. A., Bardehle, S., Tognatta, R., Dean, T., Acevedo, R. M., Cabriga, B., … Akassoglou, K. (2021). Microglial Gi-dependent dynamics regulate brain network hyperexcitability. *Nature Neuroscience*, *24*(1), Article 1. https://doi.org/10.1038/s41593-020-00756-7

Neher, J. J., Neniskyte, U., Hornik, T., & Brown, G. C. (2014). Inhibition of UDP/P2Y6 purinergic signaling prevents phagocytosis of viable neurons by activated microglia in vitro and in vivo. *Glia*, *62*(9), 1463–1475. https://doi.org/10.1002/glia.22693

Nimmerjahn, A., Kirchhoff, F., & Helmchen, F. (2005). Resting Microglial Cells Are Highly Dynamic Surveillants of Brain Parenchyma in Vivo. *Science*, *308*(5726), 1314–1318. https://doi.org/10.1126/science.1110647

Paolicelli, R. C., Bolasco, G., Pagani, F., Maggi, L., Scianni, M., Panzanelli, P., Giustetto, M., Ferreira, T. A., Guiducci, E., Dumas, L., Ragozzino, D., & Gross, C. T. (2011). Synaptic Pruning by Microglia Is Necessary for Normal Brain Development. *Science*, *333*(6048), 1456–1458. https://doi.org/10.1126/science.1202529

Parkhurst, C. N., Yang, G., Ninan, I., Savas, J. N., Yates, J. R., Lafaille, J. J., Hempstead, B. L., Littman, D. R., & Gan, W.-B. (2013). Microglia promote learning-dependent synapse formation through BDNF. *Cell*, *155*(7), 1596–1609. https://doi.org/10.1016/j.cell.2013.11.030

Pozner, A., Xu, B., Palumbos, S., Gee, J. M., Tvrdik, P., & Capecchi, M. R. (2015). Intracellular calcium dynamics in cortical microglia responding to focal laser injury in the PC::G5-tdT reporter mouse. *Frontiers in Molecular Neuroscience, 8*, 12. doi:10.3389/fnmol.2015.00012

Prager, O., Kamintsky, L., Hasam-Henderson, L. A., Schoknecht, K., Wuntke, V., Papageorgiou, I., Swolinsky, J., Muoio, V., Bar-Klein, G., Vazana, U., Heinemann, U., Friedman, A., & Kovács, R. (2019). Seizure-induced microvascular injury is associated with impaired neurovascular coupling and blood–brain barrier dysfunction. *Epilepsia*, *60*(2), 322–336. https://doi.org/10.1111/epi.14631

Puttachary, S., Sharma, S., Tse, K., Beamer, E., Sexton, A., Crutison, J., & Thippeswamy, T. (2015). Immediate Epileptogenesis after Kainate-Induced Status Epilepticus in C57BL/6J Mice: Evidence from Long Term Continuous Video-EEG Telemetry. *PLoS ONE*, *10*(7), Article 7. https://doi.org/10.1371/journal.pone.0131705

Racine, R. J. (1972). Modification of seizure activity by electrical stimulation: II. Motor seizure. *Electroencephalography and Clinical Neurophysiology, 32*(3), 281–294. https://doi.org/10.1016/0013-4694(72)90177-0

Rappold, P. M., Lynd-Balta, E., & Joseph, S. A. (2006). P2X7 receptor immunoreactive profile confined to resting and activated microglia in the epileptic brain. *Brain Research*, *1089*(1), 171–178. https://doi.org/10.1016/j.brainres.2006.03.040

Rogers, J. T., Morganti, J. M., Bachstetter, A. D., Hudson, C. E., Peters, M. M., Grimmig, B. A., Weeber, E. J., Bickford, P. C., & Gemma, C. (2011). CX3CR1 deficiency leads to impairment of hippocampal cognitive function and synaptic plasticity. *The Journal of Neuroscience: The Official Journal of the Society for Neuroscience*, *31*(45), 16241–16250. https://doi.org/10.1523/JNEUROSCI.3667-11.2011

Schafer, D. P., Lehrman, E. K., & Stevens, B. (2013). The "Quad-partite" Synapse: Microglia-Synapse Interactions in the Developing and Mature CNS. *Glia*, *61*(1), 24–36. https://doi.org/10.1002/glia.22389

Scharfman, H. E. (2007). The Neurobiology of Epilepsy. *Current Neurology and Neuroscience Reports*, *7*(4), 348–354.

Sharma, S., Puttachary, S., & Thippeswamy, T. (2019). Glial source of nitric oxide in epileptogenesis: A target for disease modification in epilepsy. *Journal of Neuroscience Research*, *97*(11), 1363–1377. https://doi.org/10.1002/jnr.24205

Sharma, S., Puttachary, S., Thippeswamy, A., Kanthasamy, A. G., & Thippeswamy, T. (2018). Status Epilepticus: Behavioral and Electroencephalography Seizure Correlates in Kainate Experimental Models. Frontiers in Neurology, 9. https://doi.org/10.3389/fneur.2018.00007

Shigemoto-Mogami, Y., Hoshikawa, K., Goldman, J. E., Sekino, Y., & Sato, K. (2014). Microglia enhance neurogenesis and oligodendrogenesis in the early postnatal subventricular zone. *The Journal of Neuroscience: The Official Journal of the Society for Neuroscience*, *34*(6), 2231–2243. https://doi.org/10.1523/JNEUROSCI.1619-13.2014

Sierra, A., Encinas, J. M., Deudero, J. J. P., Chancey, J. H., Enikolopov, G., Overstreet-Wadiche, L. S., Tsirka, S. E., & Maletic-Savatic, M. (2010). Microglia Shape Adult Hippocampal Neurogenesis through Apoptosis-Coupled Phagocytosis. *Cell Stem Cell*, *7*(4), 483–495. https://doi.org/10.1016/j.stem.2010.08.014

Sipe, G. O., Lowery, Tremblay, M.-È., Kelly, E. A., Lamantia, C. E., & Majewska, A. K. (2016). Microglial P2Y12 is necessary for synaptic plasticity in mouse visual cortex. *Nature Communications*, *7*(1), 10905. https://doi.org/10.1038/ncomms10905

The Jackson Laboratory. C57BL/6J. (2024). Retrieved February 13, 2024, from https://www.jax.org/strain/000664

The Jackson Laboratory. CX[3]CR-1[GFP]. (2024). Retrieved February 13, 2024, from https://www.jax.org/strain/005582

Thurman, D. J., Beghi, E., Begley, C. E., Berg, A. T., Buchhalter, J. R., Ding, D., Hesdorffer, D. C., Hauser, W. A., Kazis, L., Kobau, R., Kroner, B., Labiner, D., Liow, K., Logroscino, G., Medina, M. T., Newton, C. R., Parko, K., Paschal, A., Preux, P.-M., … ILAE Commission on Epidemiology. (2011). Standards for epidemiologic studies and surveillance of epilepsy. *Epilepsia*, *52 Suppl 7*, 2–26. https://doi.org/10.1111/j.1528-1167.2011.03121.x

Tito, M., Cabrerizo, M., Ayala, M., Jayakar, P., & Adjouadi, M. (2009). Seizure Detection: An Assessment of Time- and Frequency-Based Features in a Unified Two-Dimensional Decisional Space Using Nonlinear Decision Functions. *Journal of Clinical Neurophysiology*, *26*(6), 381. https://doi.org/10.1097/WNP.0b013e3181c29928

Tremblay, M.-È., Lowery, R. L., & Majewska, A. K. (2010). Microglial interactions with synapses are modulated by visual experience. *PLoS Biology*, *8*(11), e1000527. https://doi.org/10.1371/journal.pbio.1000527

Tse, K., Puttachary, S., Beamer, E., Sills, G. J., & Thippeswamy, T. (2014). Advantages of Repeated Low Dose against Single High Dose of Kainate in C57BL/6J Mouse Model of Status Epilepticus: Behavioral and Electroencephalographic Studies. *PLOS ONE*, *9*(5), Article 5. https://doi.org/10.1371/journal.pone.0096622

Umpierre, A. D., & Wu, L.-J. (2021). How Microglia Sense and Regulate Neuronal Activity. *Glia*, *69*(7), 1637–1653. https://doi.org/10.1002/glia.23961

Umpierre, A. D., Bystrom, L. L., Ying, Y., Liu, Y. U., Worrell, G., & Wu, L.-J. (2020). Microglial calcium signaling is attuned to neuronal activity in awake mice. *eLife*, *9*, e56502. https://doi.org/10.7554/eLife.56502

Vaillend, C., Mason, S. E., Cuttle, M. F., & Alger, B. E. (2002). Mechanisms of neuronal hyperexcitability caused by partial inhibition of Na+-K+-ATPases in the rat CA1 hippocampal region. *Journal of Neurophysiology*, *88*(6), 2963–2978. https://doi.org/10.1152/jn.00244.2002

Vezzani, A., Aronica, E., Mazarati, A., & Pittman, Q. J. (2013). Epilepsy and brain inflammation. *Experimental Neurology*, *244*, 11–21. https://doi.org/10.1016/j.expneurol.2011.09.033

Wake, H., Moorhouse, A. J., Jinno, S., Kohsaka, S., & Nabekura, J. (2009). Resting Microglia Directly Monitor the Functional State of Synapses In Vivo and Determine the Fate of Ischemic Terminals. *The Journal of Neuroscience*, *29*(13), 3974–3980. https://doi.org/10.1523/JNEUROSCI.4363-08.2009